40. CIE, *CIE 1988 2° Spectral Luminous Efficiency Function for Photopic Vision*, Vienna, 1990.

41. W. D. Wright, *Trans. Opt. Soc.* **30**, 141–161 (1928–29).

42. J. Guild, *Philos. Trans. R. Soc. A* **230**, 149–187 (1931).

43. R. M. Boynton, *J. Opt. Soc. Am. A* **13**, 1,609–1,621 (1996).

44. W. S. Stiles and J. M. Burch, *Optica Acta* **6**, 1–26 (1959).

45. A. R. Robertson, *Color Res. Appl.* **2**, 7–11 (1977).

46. A. R. Robertson, *Color Res. Appl.* **15**, 167–170 (1990).

47. R. S. Berns, *AIC Color 93*, Budapest, 1993.

48. CIE, *Industrial Color-Difference Evaluation*, Vienna, 1995.

49. S. S. Stevens, *Science* **133**, 80–86 (1961).

50. H. Pauli, *J. Opt. Soc. Am.* **36**, 866–867 (1976).

51. F. J. J. Clarke, R. McDonald, and B. Rigg, *J. Soc. Dyers Colourists* **100**, 128–132 (1984).

52. CIE, *The CIE 1997 Interim Colour Appearance Model (Simple Version), CIECAM97s*, Vienna, 1998.

HUMAN VISUAL SYSTEM — IMAGE FORMATION

AUSTIN ROORDA

University of Houston College of Optometry
Houston, TX

INTRODUCTION

The ultimate stage in most optical imaging systems is the formation of an image on the retina, and the design of most optical systems takes this important fact into account. For example, the light output from optical systems is often limited (or *should* be limited) to the portion of the spectrum to which we are most sensitive (i.e., the visible spectrum). The light level of the final image is within a range that is not too dim or bright. Exit pupils of microscopes and binoculars are matched to typical pupil sizes, and images are often produced at a suitable magnification, so that they are easily resolved. We even incorporate focus adjustments that can adapt when the user is near- or farsighted. Of course, it is understandable that our man-made environment is designed to fit within our sensory and physical capabilities. But this process is not complete. There is still much to know about the optical system of the human eye, and as we increase our understanding of the eye, we learn better ways to present visual stimuli, and to design instruments for which we are the end users.

This article focuses on the way images are formed in the eye and the factors in the optical system that influence image quality.

THE OPTICAL SYSTEM OF THE EYE

The optical system of the eye is composed of three main components, the cornea, the iris, and the lens (Fig. 1). The structures of these three components are complex, and their description could fill volumes. Discussion in this article is limited to their optical properties, and the
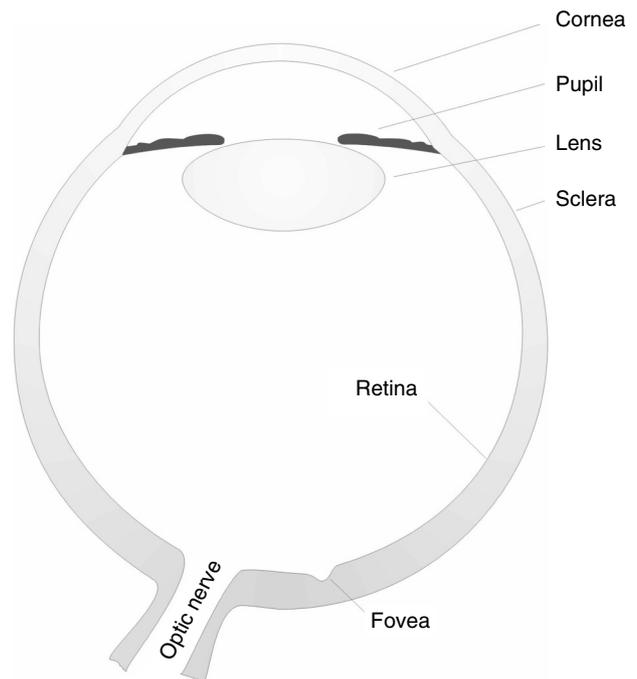

Figure 1. Schematic of the eye.

anatomy is discussed only to the extent to which it impacts image quality.

Cornea

The cornea is the transparent first surface of the eye. It is an extension of the sclera, which is the tough, white outer shell of the eye. The transparency of the cornea is facilitated by the regular arrangement of the layers of collagen fibers that comprise most of the corneal thickness (1). Periodic closures of the eyelid maintain a thin tear film on the cornea's external surface, which ensures a smooth refracting surface. However, changes in the tear film give rise to scattering and small changes in optical aberrations (2,3).

The cornea is about 0.5 to 0.6 mm thick at its center, it has a mean refractive index of about 1.376 and its first surface has a radius of curvature of about 7.7 mm. Combining this with a back surface whose a radius is about 6.8 mm gives the cornea a total power of roughly 43 diopters. Because the cornea accounts for most of the power of the eye, it follows that it is also a key contributor to aberrations of the eye. The high magnitude of aberrations that might have existed in the cornea is reduced by virtue of its conic, rather than spherical shape. The slight flattening of the corneal curvature toward the periphery reduces the amount of spherical aberration to about one-tenth of that in spherical lenses of similar power (4). But corneal shapes vary and give rise to astigmatism and higher order aberrations (5,6). Laser refractive surgery induces corneal shape changes that may correct the mean defocus error but often leave large amounts of aberration (7–9). These postsurgical corneal aberrations have been correlated with losses in visual performance (10,11).

Pupil

The pupil serves two main optical functions. It limits the amount of light that reaches the retina, and it alters the numerical aperture of the eye's image system. Because of aberrations in the eye (see later section), the biggest pupil does not necessarily provide the best image quality. The optimal pupil size is criterion dependent, but for imaging the important spatial frequencies that humans use, the optimal pupil size is between 2 and 3 mm in diameter (12−14) (see later section for more discussion). Because the pupil is between the cornea and lens, it acts as a true aperture stop, which means that changing its size does not affect the field of view of the eye. This configuration limits off-axis aberrations and also gives the eye a field of view that spans nearly the full hemisphere.

Lens

The lens is positioned immediately behind the iris. The lens in the eye adds another 20−30 diopters to the optical system. It is held in place near its equator via zonules attached to the ciliary body. The tension on the zonules is relaxed by contraction of the ciliary muscle. This action increases lens curvatures making the eye focus, or "accommodate", on near objects (15). Tension on the zonules increases by relaxing the ciliary muscle, thereby flattening the lens and allowing the eye to focus on distant objects. The lens tends to harden as it ages, which diminishes its ability to change shape (16). This, combined with other lenticular and extralenticular factors, such as increasing lens size, the changing location of the insertion points of the zonules, and the aging of the ciliary muscle [see (17) for a review], results in a loss of accommodation in a condition called "presbyopia", as shown in Fig. 2 (18,19).

The crystalline lens is composed of multiple layers of long, lens fiber cells that originate from the equator and stretch toward the poles of the lens. At the point where the cells meet, they form suture patterns. In nonprimate species, these suture patterns have simple shapes, for example a "Y", whose orientations are the same in each new layer, making it easily visible in the isolated lens (20). In the human, the embryonic eye has "Y" sutures, but as the eye ages, the suture patterns in the new layers become increasingly more complex, resulting in a lens whose suture patterns have a starlike appearance (21). Some scatter and refractive changes occur at the suture points, especially along the optical axis of the lens (21).

Crystalline layers in the lens continue to form throughout life, and the lens continues to grow with age. The development pattern gives rise to a crystalline lens that has a gradient refractive index (22). Since the gradient index was first discovered, it has been the topic of much speculation and research (15,23,24). In simpler lenses, the gradient index of refraction can be determined by optical means [ellipsoidal rat lens (25) and the spherical fish lens (26)]. The exact form of the gradient in the human eye is still unknown, but its index peaks in the center at about 1.415 and drops off slowly at first and then quickly near the surface to a value of about 1.37 (27). Whether this gradient is by design or reflects the natural properties of biological tissue is arguable, but it cannot be denied
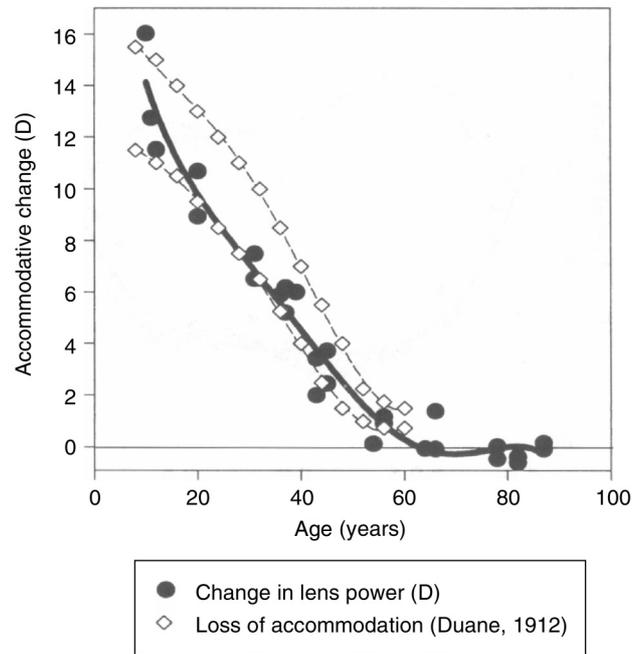
Figure 2. The ability of the lens to accommodate to different object distances decreases as it ages. By the age of 58, essentially all accommodative ability is lost. Shown here are data showing excellent agreement between a subjective test more than 1,000 eyes by Duane and objective results from optical measurements on the isolated human crystalline lens by Glasser et al. (18) [Reproduced from Fig. 5 in (18)].

that this gradient index design is far superior to a lens of similar shape that has a homogenous refractive index. First, it has been shown that the gradient refractive index creates a lens that has better optical properties than a homogenous lens (28). Second, although the gradient index crystalline lens has a peak refractive index at its core of about 1.41, a homogenous lens would require an index of refraction that is higher than the peak of the gradient, typically around 1.43 (22,29). In addition, the lower refractive indexes minimize reflection and scattering losses, particularly at the lens−aqueous and lens−vitreous interfaces.

Relative Orientation of the Components

The optical elements described work in concert to create an image on the retina. But the individual components alone cannot be analyzed without knowing their locations with respect to each other. Their approximate locations are shown in Fig. 1, but these locations vary among individuals. The optical axis of the eye would be a line joining the centers of curvature of all the optical surfaces. These points, however, do not line up, and a true optical axis does not exist. Nonetheless, one can identify an axis, called the *best optical axis*, that most closely approximates the eye's optical axis (30). The values that one finds for the tilt and decentrations of the optical components depend on the selection of this best optical axis (31,32). Even if the optics were perfectly aligned, the fact that the fovea is positioned away from this best optical axis forces us to view obliquely though the eye's optics.

An appropriate and convenient axis that can be used for the optical system of the eye is the *line of sight*, which is defined as the ray that passes through the center of the entrance pupil and strikes the fovea (the area of the retina that has the highest density of cone photoreceptors that is used for high acuity vision) (33). In other words, the line of sight is the chief ray of the bundle of rays from any object that focuses on the fovea. The line of sight can be determined quite easily in a lab setting, and it also has functional importance for vision. In the human eye, the fovea is located away from the location where the best optical axis intersects the retina. The angle between the line of sight and the best optical axis is called *angle alpha*. Angle alpha is variable, but, on average, it is displaced about 5° in the temporal direction. Based on this configuration, if the eye's best optical axes were pointing straight forward, the eyes' lines of sight would meet at a distance of 34.2 cm (assuming a distance of 60 mm between the eyes).

Changes in the Eye as It Ages

Everything in the human body change as it ages. It is not surprising that the optics of the eye and retinal image quality also change. Early aberration measurements (34) have shown that young eyes have more negative or overcorrected spherical aberrations. As the eye ages, the prevalence of positive spherical aberration tends to increase. Similar trends have been observed in the primate isolated crystalline lens (18), an optical component that continues to grow as it ages (16,35,36). This continual growth is reflected in Fig. 3, which shows the weight of the lens as a function of age. Constant environmental changes, eye growth, and age also change the corneal topography as it ages (37). It is reported that the lens and the cornea mutually compensate for the aberrations that the other imposes (38), but it is suspected that this balance is disrupted by the changing properties of each element as age increases.

IMAGE FORMATION IN THE EYE

The Mathematics of Image Formation

Even though the optical system of the eye is complex, the process of image formation can be simplified by adopting a "black box" approach to the problem. If we know how the wave front of a parallel beam is altered in a given direction, then we can predict how the image will be formed. This approach focuses on the image-forming properties of the optical system as a whole, rather than on analyzing the physical and optical properties of every component in the system. To date, this has been the most successful approach for studying image quality in the human eye. To begin, we must first establish a coordinate system (Fig. 4).

The mathematics of image formation will be based on the assumption that we have managed to measure how light has been changed by passing through the optics of the eye. The techniques for this measurement are outside the scope of this article, but the reader is referred to the following references to learn more about subjective methods (39–42) and about objective methods (2,14,43,44)
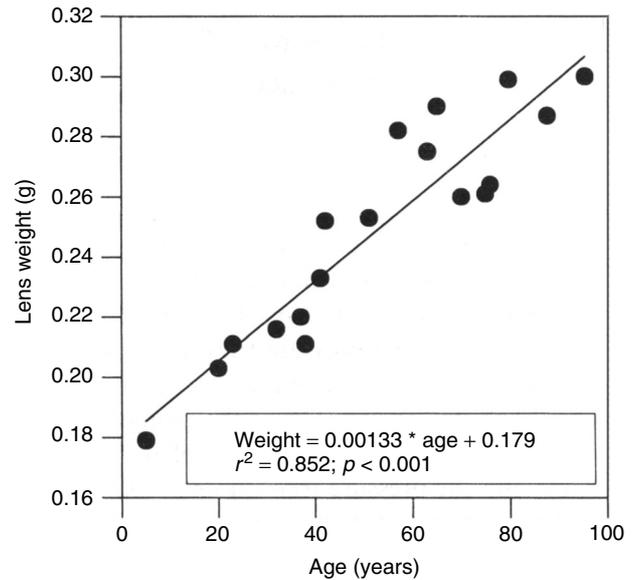
Figure 3. This graph shows the clear trend of increasing weight in the human crystalline lens as it ages, indicating an increase in lens size. Although the lens continues to grow, it does nonlinearly. For example, lens equatorial diameter does not change with age (148) [Reproduced from Fig. 3 in (16)].
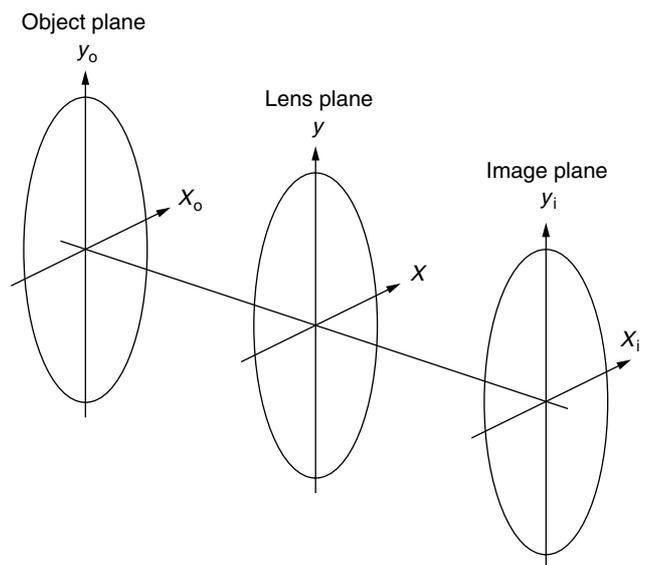
Figure 4. The standard coordinate system shown here will be used for all mathematical analyses in this article.
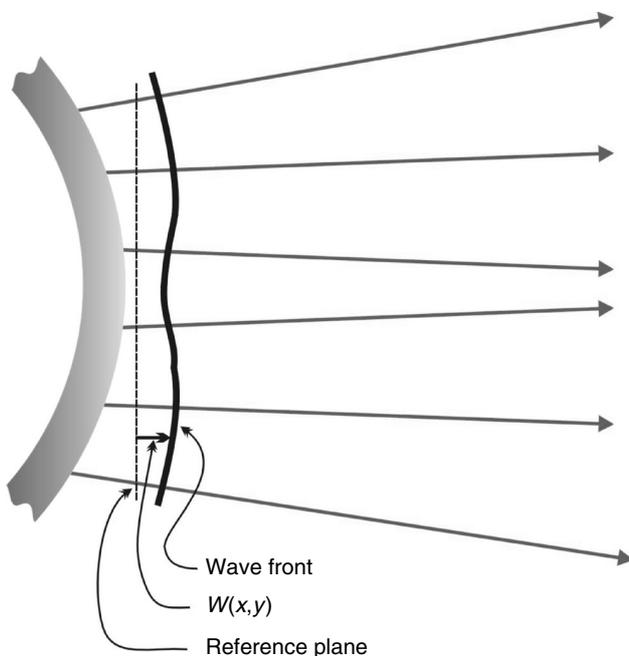
for measuring wave aberrations. The way light is changed by the optical system of the eye can be represented by the complex pupil function:

$$P(x,y) \cdot e^{-i(2\pi/\lambda)W(x,y)}. \tag{1}$$

The pupil function has two components, an amplitude component $P(x,y)$ and a phase component that contains the wave aberration $W(x,y)$. The amplitude component $P(x,y)$ defines the shape, size, and transmission of the optical system. The most common shape for the aperture

function is a *circ* function that defines a circular aperture. The size is simply the size of the pupil that the pupil function defines. A *circ* function may not always be the correct choice. For example, off-axis imaging would employ an elliptical aperture function. A clear optical system would have a value of unity at all points across the pupil function. To model variable transmission, one represents the pupil function as the fraction of transmitted light as a function of pupil location. Variable transmission may arise because of absorption in the lens. Variable transmission can also be used to model the way the eye "sees" by incorporating phenomena like the Stiles–Crawford effect (45) (see later section). In this case, the amplitude component of the pupil function takes the form of a Gaussian function (45). Another reason to use a nonuniform aperture function is to model the effect of a nonuniform beam entering or exiting the eye.

The wave aberration $W(x,y)$ defines how the phase of light is affected as it passes through the optical system. The wave front is a line that joins every point on a wave that has the same phase (see Fig. 5). In other words, it is a surface that joins the leading edges of all rays at some instant. The wave aberration is defined as the deviation of this wave front from a reference surface. The reference surface is commonly defined as a surface of curvature near the wave front whose origin is located at the Gaussian image point (where the light would be focused if the eye were perfect). If the Gaussian image is at infinity, then it follows that the reference surface is a plane. For the human eye, the natural choices for the reference surface would be a sphere whose center of curvature is at the photoreceptor

inner segments in the retina (choose the fovea for line-of-sight measurements) or at infinity for light emerging from the eye. Using such a reference sphere, departures from emmetropia (corrected vision) would appear as residual defocus and astigmatic shapes in the wave front.

The wave aberration is often defined mathematically by a series of polynomials. Common choices are the Seidel polynomials, but these can define only a limited range of aberrations. Another choice is the Taylor polynomials, which can be used to define any surface as long as enough orders are used (39). Currently, the most popular choice of polynomials is Zernike polynomials because they have convenient properties that simplify the analysis of wave aberrations (46). These polynomials can also be used to represent any surface, and the quality of the fit is limited only by the number of polynomial terms that are used.

To be complete, there is more than one wave aberration because the optics of the eye are birefringent. The birefringence of ocular structures is discussed later.
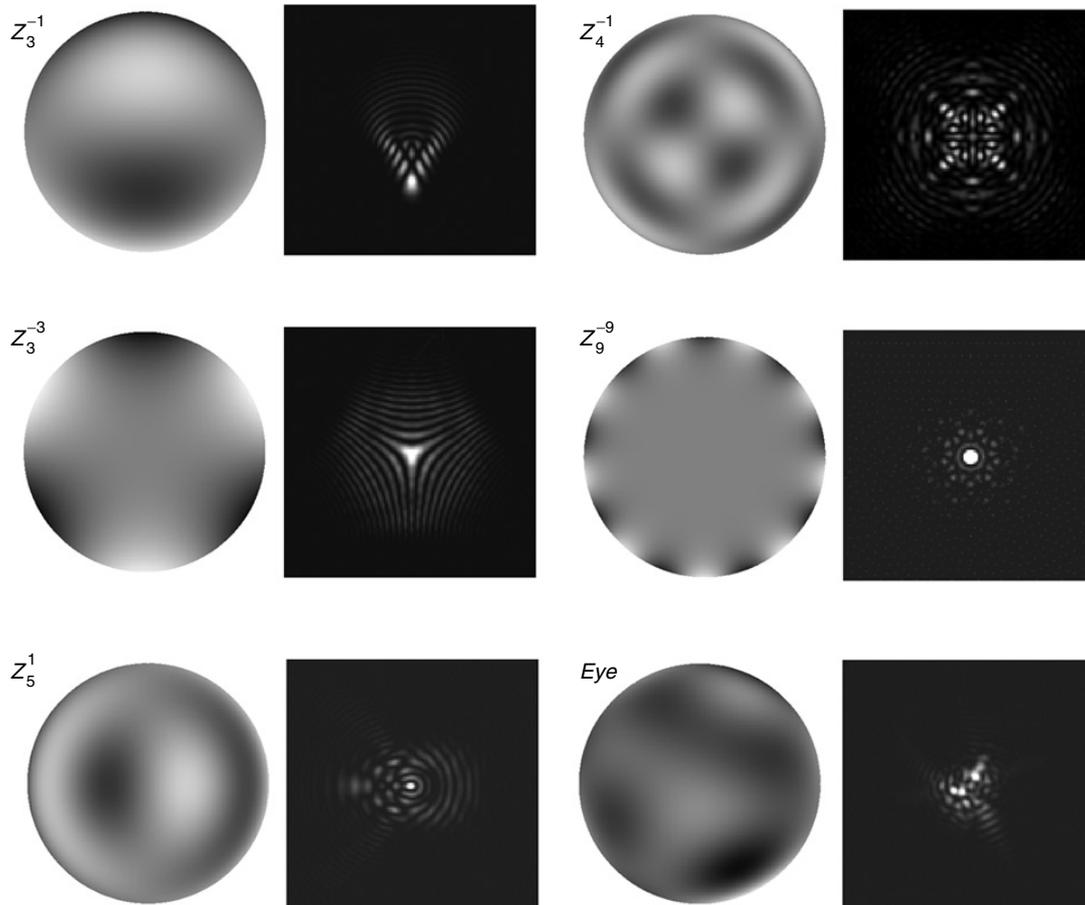
Once the nature of the light emerging from the optical system is known, optical image formation in the eye becomes relatively straightforward. The mathematics of image formation begins with the computation of the point-spread function (PSF), which is the image of a point source formed by the optical system. The PSF can be computed using the Fraunhofer approximation (for PSFs near the image plane) (47):

$$\text{PSF}(x_i, y_i) = K \cdot \left| FT\left\{ P(x,y) \cdot e^{-i(2\pi/\lambda)W(x,y)} \right\} \right|^2, \qquad (2)$$

where FT represents the Fourier transform operator and K is a constant. The actual Fourier transform is not discussed in this article. Once the concepts are understood, computations like the Fourier transform can be done numerically by using one of many common software packages such as Matlab™.

Representation of the Wave Aberration

In this section, we will limit the polynomial description of wave aberrations to Zernike polynomials (see Fig. 6). There are various forms and orders of the Zernike polynomials, but recently a committee has undertaken the task of coming up with a standard and acceptable form for use in vision (48). Any other representation of the wave aberration will work also. To predict optical quality in the human eye, it is important that to anchor the wave aberration to a precise location in the eye. It is common to choose the geometric center of the entrance (and exit) pupil as the point of origin, but in the human eye, the pupil does not always dilate symmetrically, and so the pupil center for a small pupil might be different from the pupil center for a large pupil (49). It is also known that the application of drugs to dilate the pupil causes asymmetrical dilation (50,51). A potentially stable landmark for describing aberrations might be the reflection of an on-axis source off the cornea when the eye is fixated along the optical axis, also called the coaxially sighted corneal reflex (32). This position is stable and independent of the pupil, but because it is not centered in the pupil, the computation of image quality is more difficult. So the selection of the origin depends

Figure 5. In a diffraction-limited optical system, the wave front takes a spherical shape (or a plane in the special case of a parallel beam). The wave front of the aberrated beam takes an irregular shape. The wave aberration is the difference between the reference wave front (which in most cases is the ideal diffraction-limited wave front) and the actual wave front.

Z_3^{-1}

Z_4^{-1}

Z_3^{-3}

Z_9^{-9}

Z_5^1

Eye

Figure 6. Selected wave aberrations and their respective far-field PSFs. Five single Zernike terms are shown, numbered according to the standard method for vision science (48). The wave front in the lower right corner is from a typical human eye over a 7-mm pupil.

on the application. In either case, the necessary data for determining retinal image quality are the wave aberration, the pupil size, and the relative shift between the origin of the wave-front description and the center of the eye's pupil (if the origin of the wave-front description is the line of sight, then these are the same).

In this article, wave aberration will be defined with respect to the geometric center of the entrance pupil.

Formation of the Retinal Image

The image of a point source on the retina is called the point-spread function (PSF). The next stage is to compute how the image of an object is blurred on the retina. One can think of the object as an array of point sources; each has its respective location, intensity, and spectral composition. In the limit where the object is small and composed of a single wavelength, the computation of the image can be simplified. Under this assumption (isoplanatism), each point on the object has the same PSF. To compute the image, first one computes the size of the image as if the imaging system were perfect (magnification = object vergence/image vergence). This is called the ideal image. Each point on that ideal image takes the form of the PSF whose shape is constant but whose intensity is scaled

by the intensity of the point. This process is called a convolution and is shown in the following equation:

$$I(x_i, y_i) = \text{PSF} \otimes O(x_i, y_i), \qquad (3)$$

where $O(x_i, y_i)$ is the ideal image of the object (corrected for magnification), PSF is the point-spread function, and $I(x_i, y_i)$ is the convolved image.

Intuitively, the process can be shown in real space, but in practice, the convolution is performed mathematically by computing the product of the Fourier transform of the ideal image with the Fourier transform of the PSF (47,52).

Calculation of Image Quality Metrics That Are Relevant for the Human Eye

No single number can be used to define image quality in the human eye. When image quality is good, numbers such as the Strehl ratio and the root mean square (rms) aberration are commonly used, but in this section, I show that these do not always work for the magnitude and type of aberrations encountered in the human eye. When aberrations are high, the rms wave aberration and the Strehl ratio no longer correlate. Figure 7a shows what happens if a typical eye that has a 6-mm pupil chooses

20/20 letters at minimum rms aberration

20/20 letters at maximum strehl ratio

Figure 7. In this figure, the aberrations of a typical human eye were calculated over a 7-mm pupil. The PSFs were calculated in the focal planes that had the minimum rms wave-front error and the focal plane that had the maximum Strehl ratio. In this example, the separation between the two was about 0.5 D of defocus. The PSFs were convolved with three 20/20 Sloan letters (5 minutes of arc per side). The image in the focal plane that had the maximum Strehl ratio is more readable than that of the minimum rms. Note that when you view such simulations, they are further blurred by the optics of your own eye. However, by viewing the figure at a close distance, the relative size of your PSF is small compared to that simulated in the figure.

the minimum rms as the optimal condition for reading the 20/20 letters on a Snellen chart. Figure 7b shows the same letters blurred by the PSF when the criterion of the highest Strehl ratio is chosen. These two focal planes are separated by more than 0.5 diopters. Similar trends are observed in many eyes, as shown in the plots of Fig. 8. To put that in perspective, 0.5 diopters is sufficient amount of defocus to warrant wearing spectacle lenses. Based on Fig. 7 alone, one might argue that the defocus that gives the highest Strehl ratio is the most relevant choice for human vision, but this may apply only to visual acuity measurements. Recent findings suggest that the image quality metrics that correlate best with subjective preference are those based on the image plane (i.e., the Strehl ratio, encircled energy) rather than the pupil plane (rms, peak-to-valley aberration) (53). In summary, the rms can be a good indicator of optical quality, but minimizing the rms does not necessarily ensure the best image quality.

Humans rarely work at the limits of their visual capability. The eye can perceive spatial frequencies as high as 50 cycles per degree, but the range of spatial frequencies that is most important for vision and that dominates the visual scene is predominantly lower. Spatial frequencies in the environment have amplitude spectra that approximately follow a $1/f$ law, where f is the spatial frequency (54,55). An image quality metric that appreciates the importance of this range of spatial frequencies might be the best choice. Best image quality might occur when the area under the modulation transfer function (MTF) is maximized for those spatial frequencies.

Two methods are commonly used to assess subjective image quality, visual acuity and contrast sensitivity. Visual acuity is a classic measure, but it tests very high spatial frequencies and may not be a meaningful measure of the quality of vision. This argument is supported by the fact that visual acuity does not correlate with typical variations in aberration until very high amounts of aberration are present (10). The contrast sensitivity function is the visual analog to the modulation transfer function, except that it combines the optics of the eye with the neural limits imposed in part by the discrete sampling array of photoreceptors (12). Although the contrast sensitivity function is a more tedious measurement to make, it reflects the quality of vision for all spatial frequencies when visual acuity tests vision only at its limits.

IMAGE QUALITY IN THE HUMAN EYE

Chromatic Aberrations

Dispersion of the refracting media in the human eye gives rise to chromatic aberration. This chromatic aberration manifests itself in two ways, longitudinal and transverse.

Longitudinal Chromatic Aberration. Longitudinal chromatic aberration refers to the change in focus as a function of wavelength. The degree of chromatic aberration is relatively constant between eyes, and there is general agreement among the measured values in the literature (33). Chromatic aberration often describes the changing power of the optical system, but it is more common to describe chromatic aberration in terms of the way it affects the refraction of the eye. This is more appropriately called the *chromatic difference of refraction*. Refraction defines the optical correction required outside the eye to correct it for focusing at infinity. It is a more clinically meaningful quantity and is easily measured by a variety of techniques. Bennett and Rabbetts published chromatic difference of refraction curves summarizing the results from a collection of studies, and it is reproduced here in Fig. 9. The graph shows that the chromatic difference of refraction is 2.2 D across the visible spectrum (from 400 to 700 nm). This implies that if the eye is properly focused on 700 nm light at infinity, 400 nm light must be at a distance of 45 cm from the eye to be in focus.

The first impression might be that this amount of chromatic aberration of the eye would be seriously deleterious for vision. After all, a refractive error of
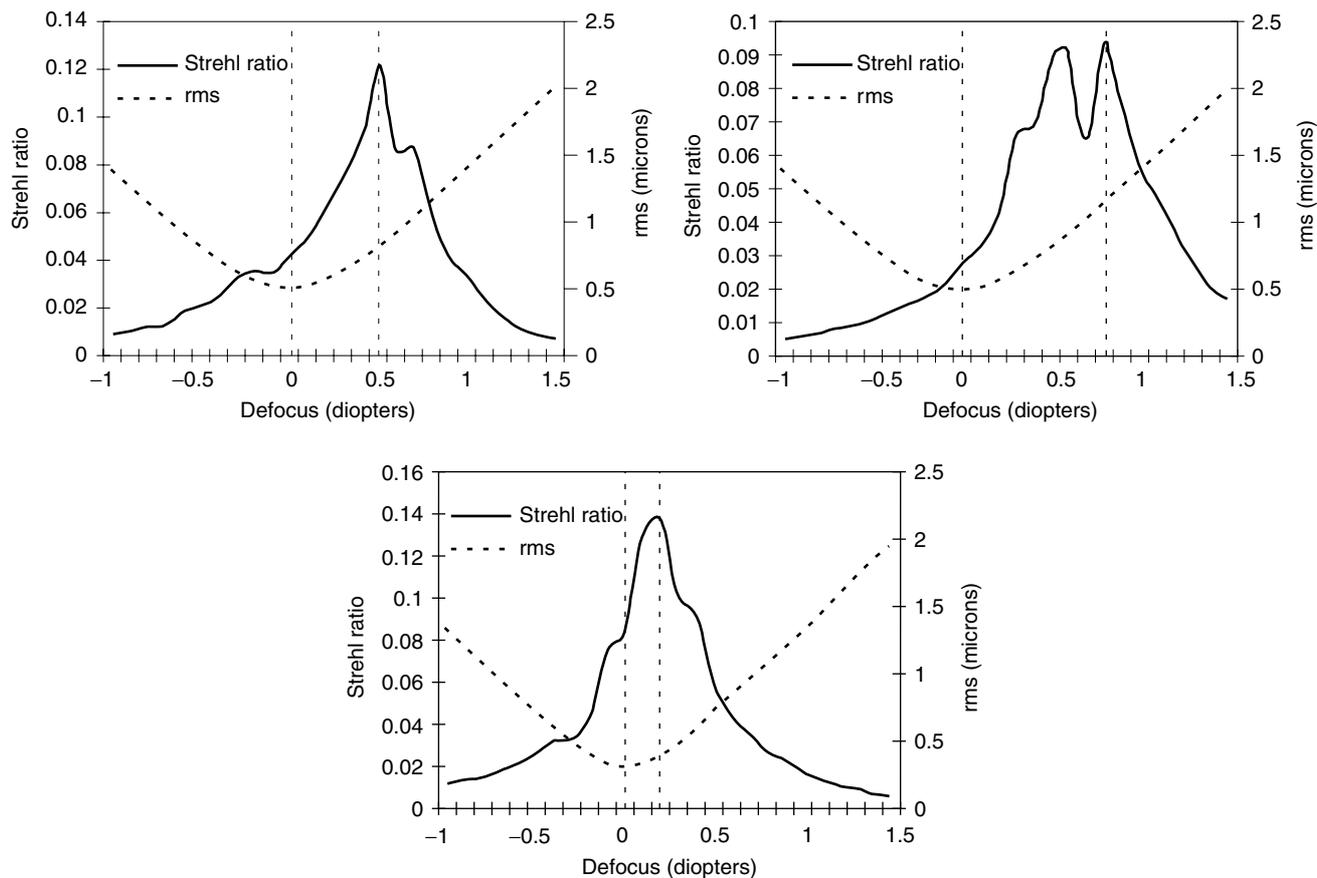
Figure 8. The aberrations of three individuals were measured over a 6-mm pupil. The rms and the Strehl ratio were calculated as a function of defocus for each eye. The graph shows that the best focal plane is criterion dependent.

0.25 D is severe enough to warrant wearing a spectacle correction. The severity of the chromatic aberration is lessened because the eye has a tuned spectral bandwidth. This is discussed in more detail later.

Of all the aberration terms that are present in the eye, the defocus is certainly not the only aberration that changes as wavelength changes. Marcos et al. showed that other aberrations, including astigmatism and spherical aberration, also change as wavelength changes, although to a lesser extent (56). Even without aberrations, diffraction itself causes changes in the image forming properties as a function of wavelength [see Eq. (2)].

Transverse Chromatic Aberration. Transverse chromatic aberration arises because of a difference of refraction in the chief ray as a function of wavelength. So, in addition to a difference in focus, chromatic aberration also gives rise to differences in the retinal location of the image as a function of wavelength.

Transverse chromatic aberration affects mainly off-axis objects. The reason for this is that the entrance pupil is axially displaced from the nodal points of the eye. The amount of off-axis transverse chromatic aberration nearly matches the sampling efficiency of the eye as a function of retinal eccentricity, so it is not a serious problem. However, the most serious effects occur at the fovea. Transverse

aberration at the fovea occurs because the nodal points do not lie along the line of sight. In other words, the foveal achromatic axis (the ray that joins the nodal points with the fovea) is not necessarily collinear with the line of sight. This aberration has been carefully measured using vernier alignment techniques (57–59). From these studies, the transverse chromatic aberration between 400 and 700 nm at the fovea was typically within 1 minute of arc but larger variations have been found in other studies (56). Because the photoreceptor sampling is very high at the fovea, any amount of transverse aberration can be a problem. The amount of transverse chromatic aberration is only slightly larger than the size of a single foveal cone, indicating that there is very little disparity between the line of sight and the achromatic axis. Nonetheless, this disparity is greater than the minimum disparity that the human eye can detect [the ability to detect tiny displacements in the alignment between two objects is called vernier acuity or hyperacuity and is about 6 seconds of arc (60)].

Monochromatic Aberrations

On-Axis Aberrations. Scientists have studied the monochromatic aberrations of the eye for the last two centuries (13,15,22,31,39–44,61–69). The on-axis aberrations of the eye refer to those aberrations that occur at the fovea of the eye. To be exact, these aberrations are those that
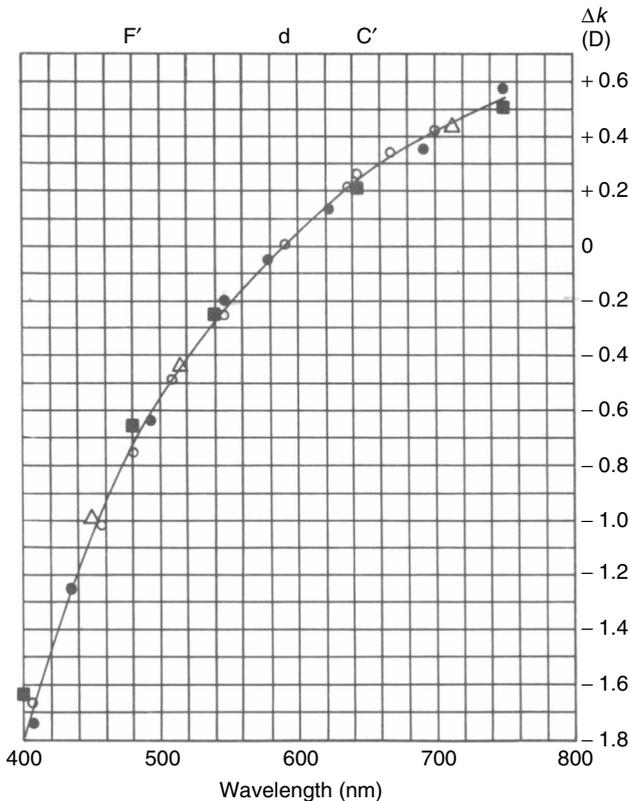
Figure 9. The chromatic aberration of the eye causes a chromatic difference of refraction. It is plotted here as the refractive error of the eye as a function of wavelength where all data are normalized to a standard wavelength of 587.6 nm. Symbols are from the following: Wald and Griffin (149), ○ Bedford and Wyszecki (150), △ Ivanoff (151), and ■ calculated results for the Gullstrand-Emsley model eye by Bennett and Rabbets (33). The line represents the mean of all the data [Reproduced from Fig. 15.5 in (33)].

occur along the line of sight, which is about 5° from the best optical axis of the eye.

Current computing technology allows us to derive and manipulate routinely the mathematical forms that represent the wave aberration of the eye. In 1977 Howland and Howland generated the first mathematical expressions that defined the total wave aberration of the eye (39). Since then, enough reports of the total aberration have been published to permit calculating the typical trends in the total aberration of the eye.

Full descriptions of ocular aberrations are still developing. To date, the largest single published study of ocular aberrations included only 55 eyes (39). In total, the published literature in which the wave aberrations are described mathematically includes a total sum of less than 300 eyes. However, the recent development of the Hartmann−Shack wave-front sensor for the human eye has allowed rapid, accurate, and objective ocular aberration measurements, and this technique is currently being used to obtain the first extensive population studies of human eye aberrations.

Table 1 shows the rms aberration drawn from studies in which the appropriate data have been published. Figure 10

is a plot of the same data. The graph shows a nearly linear increase in rms as pupil size increases. In general, there is good agreement among the separate studies.

It is now well known that the aberrations of the human eye have a large amount of interindividual variation. Do the same variations exist in the degree of aberrations? A list of rms aberrations as a function of pupil size reveals that, on average, aberrations increase as pupil size increases. The variation is not small, however. In a study of 14 subjects, Liang and Williams found a range of rms errors of 0.92 to 0.26 microns for a 7.3-mm pupil (14). These variations have significant impact on image quality and are likely factors contributing to variability in humans' best-corrected visual acuity.

The only trend that has been found in the higher order aberrations is a tendency for the relaxed eye to have an average spherical aberration component that is positive (4,14). No trends have been found in any other aberrations. Although the on-axis measurements are actually displaced from the best optical axis by about 5° (angle alpha), no investigator has found that any systematic off-axis aberrations such as coma exist at the fovea.

Table 1. Plot of Average RMS Aberration for Human Eyes Drawn from Selected Papers

Pupil Size	RMS Aberration (microns)	Standard Dev. (microns)	Number of Eyes	Ref.
4	0.210028	0.060594	5	68
6.7	0.45	0.1	4	80
5.4	0.241885	0.03894	2	2
7.3	0.47	0.19	14	14
3.4	0.207		12	14
5	0.162	0.041503	11	44
7.33	0.83	0.05	8	85
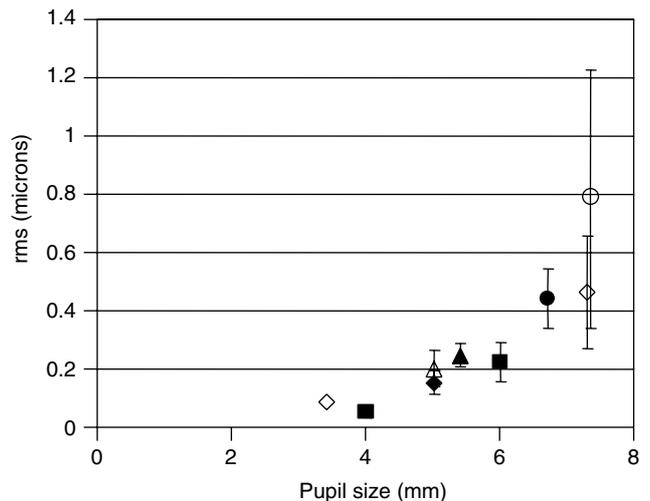
Figure 10. Each point on the graph represent results from a different study. Symbols are from the following studies: ○ He et al. (85); ◇ Liang and Williams (14); ● Navarro et al. (80); ▲ Liang et al. (2); △ Iglesias et al. (152); ◆ Walsh et al. (44); ■ Calver et al. (153). The plots shows that the rms aberrations increase as pupil size increases.

Off-Axis Aberrations. Like most optical systems, the optical quality of the eye degrades as the image moves away from the best optical axis. The most dominant off-axis aberration is astigmatism and its associated curvature of field. Compensation for curvature of field is facilitated by a curved image plane, or retina (22), so that in most eyes, the retina sits between the sagittal and tangential image planes. Objective techniques to measure off-axis astigmatism have found a nearly parabolic increase in astigmatism to between 4 and 5 diopters at 40° eccentricity from the fovea (70–73). Earlier refractometric measurements show similar characteristics at slightly less magnitude (74–77).

As expected, other aberrations are also present off-axis, but these aberrations have yet to be completely characterized. Double-pass techniques have been effective for measuring the MTF of the eye, but the ability to extract the magnitude of odd aberrations is impossible (70,78,79). Navarro et al. used an objective ray-tracing model to estimate coma and other high-order aberrations in the periphery (80). In both cases, the amount of coma, measured off-axis, was significantly greater than that measured at the fovea. Overall, Navarro et al. found that the rms of higher order aberrations (5-mm pupil corrected for defocus and astigmatism at all eccentricities) increased linearly from 0.45 microns at the fovea to 1.13 microns at 40°. Incidentally, Rempt et al. (76) were the first to observe the effects of off-axis coma by using a retinoscope, but they did not identify it as caused by coma. They discussed the common occurrence of the "sliding-door" appearance of the retinoscopic reflex at off-axis locations, which is a phenomenon that can be entirely explained by the presence of coma (81).

How much degradation in vision is expected from these off-axis aberrations? As it turns out, off-axis aberrations are not that problematic for vision because the detail we can see is most limited by the coarseness of the sampling array in the retina. This will be discussed more later. But, even though retinal sampling imposes the limit on resolution in the periphery, the blur due to off-axis aberrations significantly reduces the amount of aliasing that might occur (71,82). This is another example that suggests an exquisite codevelopment of the sampling and imaging capabilities of the human eye.

Aberrations and Accommodation. During accommodation, the shape of the lens is changed by application and relaxation of zonular tension at its equator, so it follows that there are associated changes in the wave aberration of the lens. The predominant result revealed in the literature has been a tendency for the spherical aberration of the eye to move in a negative direction as it accommodates (34,62,63,83–85), although large interindividual variability was observed. Some subjects showed no dependency on aberration with accommodation, whereas a subset of subjects experienced a reversal of the sign of the spherical aberration. The He et al. study found that the overall aberrations (measured as the rms wave aberrations) decreased to a minimum then increased from further accommodation (85). They found that for most eyes there was an accommodative state for which the aberrations were at a minimum and that this accommodative state was typically near the resting state of accommodation. The resting state of accommodation also called the dark focus, is where the unstimulated eye focuses (for example, if left in a dark room). It is typically at an accommodative state of about 2 diopters or at a focusing distance of about 50 cm.

Studies of the isolated human lens have shown similar changes toward more negative spherical aberration from accommodation (18,86). It is important to add that the change in aberration from accommodation is roughly of the same magnitude as the total aberrations in any accommodation condition (87). This result has two important implications. First, because the change in aberration from accommodation is high, the lens must be a significant contributor to the total aberration of the eye. Secondly, this result means that a fixed aberrational correction in the eye applies only for a single accommodative state and any benefit will be diminished in a departure from that optimal state. This is important, given that refractive surgical techniques (e.g. LASIK) are working toward the possibility of improved best-corrected vision by correcting higher order aberrations (88).

Sources of Aberration in the Eye. Few studies have determined the relative contributions of the various optical components to the total aberration of the eye. The reason for the lack of studies has been that techniques to measure the total aberration of the eye and techniques to compute the aberration of the cornea and lens are still maturing (18,38,89). For this reason, this section will report on some results for which full papers have yet to be published. The main contributors to the total aberration of the eye are definitely the cornea and the lens and their relative locations with respect to the pupil. In the cornea, the main contributions are from the outer surface, which has most of the corneal power.

As stated in the previous section, the change in aberration from accommodation is roughly of the same magnitude as the total aberrations in any accommodation condition (90). So the lens is not a minor contributor.

A recent study by Artal et al. measured the internal ocular surfaces in living eyes by using a Hartmann–Shack wave-front sensor. The aberrations of the cornea were neutralized by immersing the cornea in water. They found that the aberrations of the internal ocular surfaces in a 4-mm pupil, were often higher than the aberrations of the whole eye and concluded that the lens in some eyes must have a compensatory effect on the aberrations of the cornea (89,91). Another study compared the aberrations of the cornea with the total aberration of the eye (92). They found only one of three eyes where the internal surfaces had a compensatory effect on the corneal aberrations. Bartsch et al. obtained slight improvements in image quality in a scanning laser ophthalmoscope after correcting for the cornea by using a contact lens. They imaged the retina using a 7-mm scanning beam (93). The Bartsch et al. results suggest that, although the lens may have a compensatory effect, the aberrations of the cornea still dominate.

In general, these early results indicate that there is some compensatory effect of the lens, but it is not present

in all eyes, and there is individual variability. Some variability of the results may be due to studies using different pupil sizes.

Aberrations and Refractive Error. Defocus is the dominant aberration in the human eye. It is also the easiest to correct. But do high refractive errors come with increased aberrations? Few studies have addressed this question to date, but several studies are currently underway, and early results suggest that high myopes tend to suffer from higher aberrations also (94), even though the one published study states otherwise (95).

These findings raise some interesting questions. For example, because the eye uses a feedback system to maintain emmetropia, then does the presence of aberrations disrupt the feedback system to an extent that leaves the eye myopic? Or, conversely, does the myopic eye lack a sufficient feedback signal to drive the correction of higher order aberrations? The relationship between refractive error and aberrations remains unknown at this time.

Scattering in the Human Eye

Scattering occurs whenever light encounters refractive index discontinuities in its path. The specific types of scattering that can occur depend on the nature of these discontinuities. In a simple example, light striking a spherical particle has a scattering profile that depends on the relationship between particle size and wavelength. Scattering from particles that are much smaller than the wavelength of light is equal in the forward and backward directions. This is called Rayleigh scattering. As the particle size increases to a size that is close to the wavelength, the scattering, called Mie scattering, is predominantly in the forward direction. Finally, when particle sizes are much greater than the wavelength, geometrical approximations can be applied, and typically all of the scattered light is in the backward direction. Relative proportions of scattered light for different scattering particle sizes are listed in Table 2.

Scattering depends on particle size with respect to wavelength, so it follows that the amount of scattered light for a fixed particle size depends on wavelength. But only a small relationship has ever been observed in the human eye (96). There is no doubt that Rayleigh scattering will exist; in fact, it has been measured in the nuclei of excised human lenses (97), but the scattering in the optics of the eye is dominated by the larger scattering particles, whose scattering has less wavelength dependence.

How scattering affects the human eye depends on the specific application. For vision, the most important type of scatter would be forward scatter. However, for retinal imaging, both forward and backward scatter affect image quality.

When scattering increases in the eye, it is primarily the amplitude of the scatter that changes, not the angular distribution of the scattered light. It has been found that the change in scatter as a function of angle follows the rule

$$\frac{L_{\text{eq}}}{E_{\text{gl}}} = \frac{k}{\theta^2} \qquad (4)$$

where L_{eq} is the equivalent veiling luminance (in cd/m^2), E_{gl} is the illuminance at the eye, k is a constant, and θ is the scattering angle (98). As shown in the equation, the profile of scattering in the eye as a function of angle follows a power law of approximately -2. This value is close to a constant, even in the presence of cataract. With regard to k, the Stiles–Holladay approximation (99,100) puts the value of this constant at 10 for a healthy eye, but more recent work has determined the important dependency of the constant on age (101,102); also see (98).

Transmission by the Human Eye

The optics of the eye are not completely transparent across the range of visible wavelengths. Even though almost all red light incident on the cornea reaches the retina, a significant fraction of light toward the blue end of the spectrum does not, and the amount of light that is absorbed changes dramatically as the eye ages.

All of the optical components, including the aqueous and vitreous, act as band-pass filters in the human eye. But the cornea and the vitrei have bandwidths that essentially exceed the visible spectrum. The lens, on the other hand, has significant absorption at the blue end of the visible spectrum, cutting off most of the

Table 2. Scattering of a Spherical Particle ($n = 1.25$) as a Function of Size and Direction of Scatter

θ	Rayleigh Regime $\rightarrow = \leftarrow$ Mie Regime						
	$a^a = \dfrac{\lambda}{100\pi}$	$a^a = \dfrac{\lambda}{10\pi}$	$a^a = \dfrac{\lambda}{2\pi}$	$a^a = \dfrac{\lambda}{\pi}$	$a^a = \dfrac{\lambda}{0.5\pi}$	$a^a = \dfrac{\lambda}{0.2\pi}$	$a^a = \dfrac{\lambda}{0.12\pi}$
0° (forward)	1.00	10,000.00	9.60×10^6	4.60×10^8	2.15×10^9	7.84×10^{10}	2.34×10^{11}
90° (sideways)	0.50	5,000.00	4.03×10^6	7.36×10^7	1.25×10^8	2.20×10^8	2.23×10^8
180° (backward)	1.00	9,800.00	6.24×10^6	3.82×10^6	1.01×10^7	1.02×10^8	2.81×10^7

$^a a$ is the diameter of the scattering particle. Scattered light in all directions is normalized to the amount of scattered light in the forward direction for the smallest particle size. All polarizations have been added for each scattering direction. The table shows that the total amount of scattered light increases but that the relative amount of backscattered light decreases as the scattering particle size increases. As the size of the scattering particles increases further, backscattering begins to dominate again (157).

light below 400 nm (103). Boettner and Wolters published a comprehensive study of the contributions of these components by directly measuring spectral transmission of freshly enucleated donor eyes (104). Their results may suffer from postmortem artifacts, but the graph is reproduced here as Fig. 11 because the data are presented in an informative way that illustrates the lens contribution relative to the other components and the cumulative effect of the absorbing tissue.

The absorbance of blue light in the crystalline lens is commonly referred to as "yellowing" of the human lens. This yellowing of the lens increases dramatically as it ages. The lens optical density toward the blue wavelengths increases by about 0.1 to 0.15 log units per decade, provided that we assume that components other than the lens change little as they age (105,106). Accelerations in this rate have been found for eyes over age 60 (106,107), and it is proposed that this increase is due to the prevalence of cataract in that age group. When eyes that had cataract were excluded from the study, it was found that a linear increase in optical density versus age was maintained (105). The optical density of the lens is highly variable. The optical density for any given age group might span 0.8 log units or more (105). Tabulated data on the lens transmission spectrum can be found in Pokorny et al. (106) or in van Norren and Vos (103). Plots of the change in lens optical density versus age can be found in Savage et al. (105) and Delori and Burns (107).

In addition to the absorbance by the optics, the retina itself has pigments that filter the light reaching the photoreceptors. The first filter arises from the blood vessels and capillaries that course through the retina and line the most anterior layers of the retina. No blood vessels lie

directly over the fovea, but in more peripheral regions, the areal coverage can be as high as 30% (108). Primary absorption in the blue end of the spectrum gives blood its red appearance but some absorption peaks also exist in the 500–600 nm spectral region. The choroid, which is posterior to the photoreceptors, is also rich in blood, which may alter the spectral properties of light scattered from the retina. The penetration of light into the choroid is reduced, however, by the presence of melanin pigment in the retinal pigment epithelium (see end of section).

The most dominant filter in the retina is a yellowish pigment in the macular region near the fovea, called the macular pigment. Incidentally, this pigment is very similar to xanthophyll in the leaves of green plants (109). The amount of macular pigment is variable between individuals and ranges in optical density from 0.21 to 1.22 (110,111). The density depends on factors such as iris pigmentation, diet, and smoking (112). The density peaks at the fovea and declines exponentially to half its peak value at an average foveal eccentricity of 0.95° (±0.4° sd) visual angle or about 285 microns, and the distribution of macular pigment is nearly symmetrical about the fovea (113).

The functional role of the macular pigment is still under debate. Some argue that the macular pigment is intended to filter out blue light (114), like an anatomical version of the yellow tinted sunglasses that are often worn by target shooters. Its role would be to increase the contrast of the retinal image by filtering out the out-of-focus blue light from the image. A more popular argument contends that the macular pigment reduces the amount of damaging blue light exposure. Reduced blue light exposure might prevent the onset of age-related macular degeneration, a disease that impacts central vision (115). Others contend that the macular pigment is simply a by-product of the increased metabolic activity that occurs in the cone-rich fovea. Whether accidental or intentional, the presence of macular pigment affects vision and reduces harmful blue light radiation.

In addition to the macular pigment, Snodderly et al. found two other yellow pigments that have lower optical density and change more slowly across the retina (116). These pigments are not expected to have a significant impact on vision because they have spectral peaks of 435 and 410 and have maximum optical densities of less than 0.05. However, they should not be ignored if one wants to infer the spectral properties of the macular pigment by comparing psychophysical responses between the periphery and the fovea. The areal distribution of the macular pigment and these other pigments are shown in Fig. 12.

Finally, there are other pigments in the eye, such as the blood in the choroid, that do not lie along the direct optical path from the object to the retina but still might affect vision via multiple scattering from deeper layers in the retina. But the eye is equipped with an optically dense, wideband, absorbing layer of melanin in the retinal pigment epithelium that lies immediately posterior to the photoreceptor layer. The retinal pigment epithelium's primary role is to maintain and nourish the photoreceptors. It is also considered responsible for
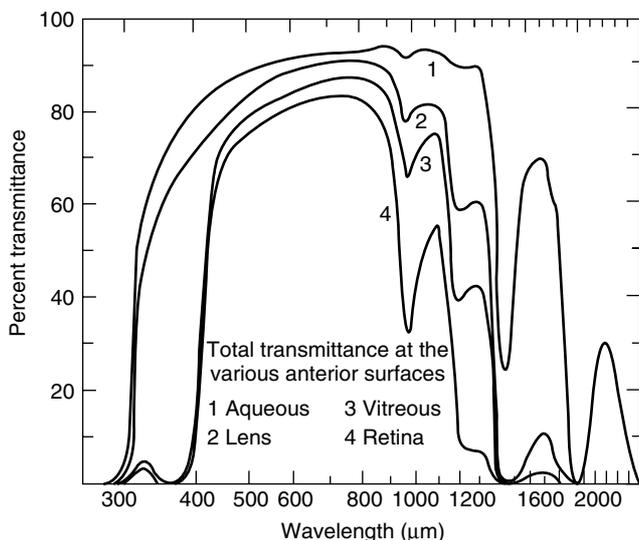
Figure 11. The spectral distribution of light that reaches the retina depends on the transmission of the components that precede it. In this plot, the successive spectra at a series of interfaces are shown. The data are drawn from young eyes and are the "direct" transmittance (i.e., the spectra were measured in the vicinity of the focal point of the eye). By the time the light reaches the retina (curve 4), it is limited to a wavelength band from 400–1,200 nm [Reproduced from Fig 7 in (104)].
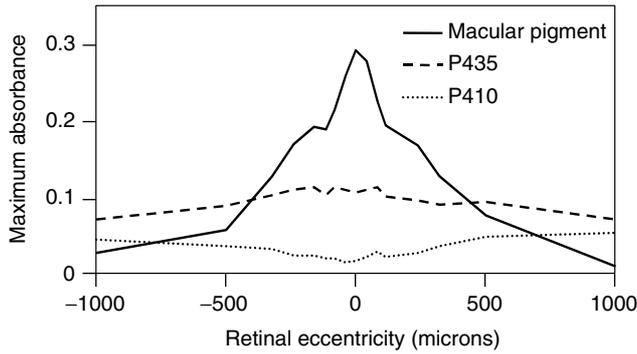
Figure 12. The concentration of some of the retinal pigments varies with retinal location. P435 and P410 are relatively uniform across the retina compared to the macular pigment, which is concentrated near the fovea [after (116)].

mopping up light that is unabsorbed by the photoreceptors. This light would otherwise penetrate and scatter from the choroidal layers. The spectra of all of the important pigments that are not part of the optical system are shown in Fig. 13.

Polarization Properties of the Ocular Optics

The speed of propagation of light in a medium depends on the structure of that medium. Some media, particularly crystalline media, can be anisotropic, that is, the atomic structure of the crystal differs in different directions. The speed of propagation in these anisotropic media depends
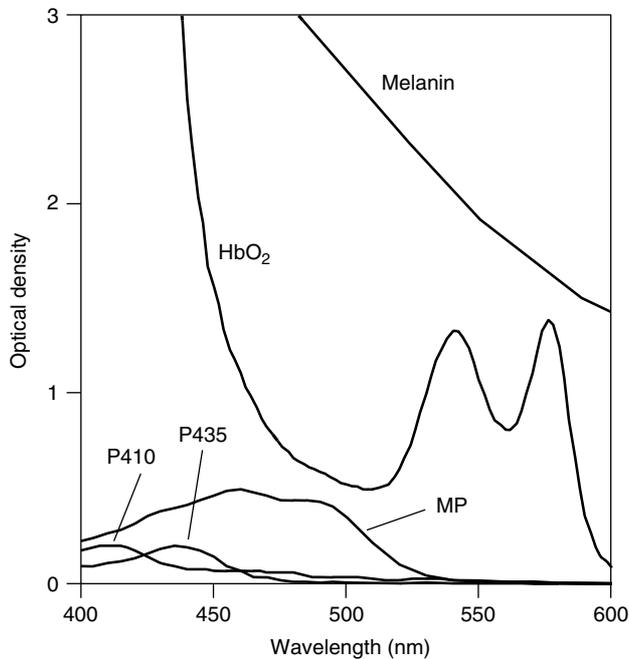
Figure 13. Plot of some of the important retinal pigments. Macular pigment, P410, and P435 are anterior to the photoreceptor layer. Hemoglobin (HbO_2) absorption occurs both anterior to and posterior to the photoreceptors in both retinal vasculature and the choroidal vasculature, respectively. Melanin resides posterior to the photoreceptors in the retinal pigment epithelium and the choroid.

on the direction of the applied electromagnetic field in relation to the crystal lattice. Thus, there can be two indexes of refraction and two possible values of the speed of propagation of light in a crystal in any given direction.

Polarization refers to the direction of the applied field perpendicular to the direction of propagation. Any polarization orientation can be expressed as the sum of two orthogonal components, and their respective directions are along the crystal axes. The two values of the speed of propagation, therefore, are associated with the mutually orthogonal polarizations of light waves.

It has been found that the human cornea has polarization-altering properties, and there have been two common models for the cornea that give rise to these properties. The first is to assume the cornea has a uniaxial structure. There is only one optical axis in a uniaxial crystal. An optical axis defines a propagative direction for which both orthogonal components of the polarization travel at the same speed. This implies that in two major polarization directions, there is no difference in the structure and there is only one light-propagative direction for which both orthogonal directions of polarization are retarded equally. That direction is normal to the corneal surface. This model, applied to the cornea, assumes that there is essentially a random orientation of the sheets of lamellae in the corneal stroma. If the optical axis is normal to the surface of the cornea at its apex, then its curved structure will give rise to polarization effects for more peripheral rays because it introduces a component in the polarization that is normal to the surface. This property was measured in the cat by Stanworth and Naylor (117). A more sophisticated and accurate model assumes that the cornea has a biaxial structure in which there are two optical axes in the crystal (118–121). In each major direction in the plane of the corneal surface, there is a different structure. In such crystals, there are two directions of light propagation for which both orthogonal components of the light travel at the same speed. The biaxial nature of the human cornea arises because of the preferred orientation (nasally downward) of the lamellar sheets in the stroma. The results of measured birefringence from a number of authors are shown in Table 3. A plot showing the polarization altering properties of the cornea from the paper of van Blokland and Verhelst is shown in Fig. 14.

Table 3. Birefringent Properties of the Cornea

Species	$n_z - n_x$	$n_y - n_x$	Ref.
Human	0.00159	0.00014	(118)
Human	0.0020	NA	(158)
Cat	0.0014	0	(117)
Bovine	NA	0.00013	(159)
Cat	0.0017	NA	(160)

$^a n_x$ is the index along the slow axis (down and nasal); n_y is the index in the orthogonal direction, tangential to the corneal surface; and n_z is the index in a direction normal to the corneal surface. The birefringence between lateral and normal ($n_z - n_x$) is about an order of magnitude greater than between n_x and n_y, which explains why some investigators like (117) were close when they assumed that the eye was simply a curved uniaxial crystal.
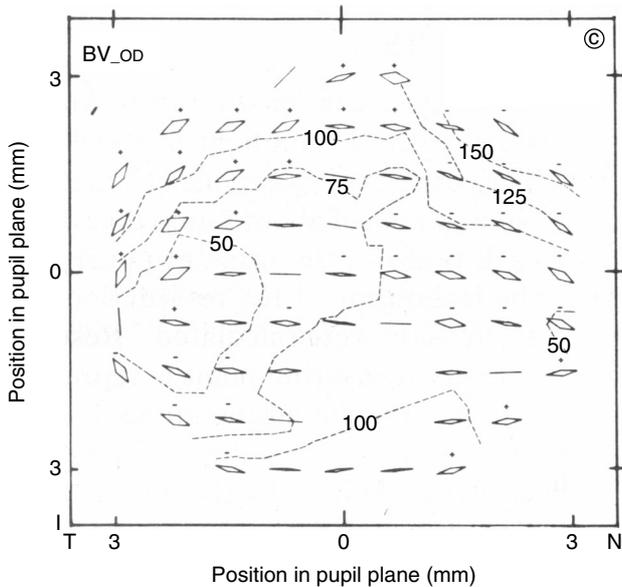
Figure 14. Birefringent properties of the cornea alter the polarization of transmitted light. This plot shows the orientation, ellipticity, and retardation after a double passage of 514-nm light through the ocular optics. The incident beam was positioned centrally, and each diamond represents a measured corneal location. The changes in ellipticity and orientation of the polarization of the emerging light are indicated by the orientation and ratio of the short to the long axes of each diamond. The contour lines represent points of equal retardation in 25-nm intervals. The plot has a saddle-shaped function, pointing nasally downward, a direction consistent with the preferred orientation of lammelar fibers that comprise the corneal stroma. [Reproduced from Fig. 1 in (118)].

How might this affect image quality in the eye? A biaxial crystal has different indexes of refraction; hence, phase errors depend on the orientation of the polarization of the light. Take, for example, the calcite crystal, one of the most birefringent structures in nature. The difference in the refracted angle between two orthogonal polarizations is 6.2°. If calcite were used in an imaging system, the PSF would be comprised of two discrete points. But the birefringence of calcite is 0.172, which is three orders of magnitude higher than that found in the cornea. Nonetheless, the effects of birefringence of the optics are likely to play a role, albeit a minor one, compared to aberrations in degrading retinal image quality (122). The difference in phase error across the cornea between two orthogonal states of polarization is less than one-tenth of a wave in the center of the cornea (118,123). Differences of about one-third of a wave have been measured at the edge of the optics (118).

Now, consider a case where one is looking through a polarizing filter at a retina that is illuminated by polarized light (laser). In this case, because the degree and orientation of the emergent light varies in its polarized state, it is conceivable that the polarizing filter will attenuate some areas of the pupil, and other areas will transmit fully. According to the figures by van Blokland and Verhelst, this attenuation can be as such as 100%. So the amplitude modulation [see equation for $P(x, y)$ in a

previous section] of the pupil will vary greatly and might give rise to a degraded (or improved) PSF (122).

The lens contributes very little to the overall polarization in the eye. Its values of birefringence (comparing radial vs. tangential index of refraction) are more than two orders of magnitude less than that found in the cornea. Bettelheim finds birefringence values in the range of 10^{-6} to 10^{-7} (124). Still, an effect of crystalline lens birefringence can be observed if one looks at an isolated lens through a pair of crossed polarizers (125). Such an example of a lens imaged though crossed polarizers is shown in Fig. 15.

RECEIVING THE RETINAL IMAGE
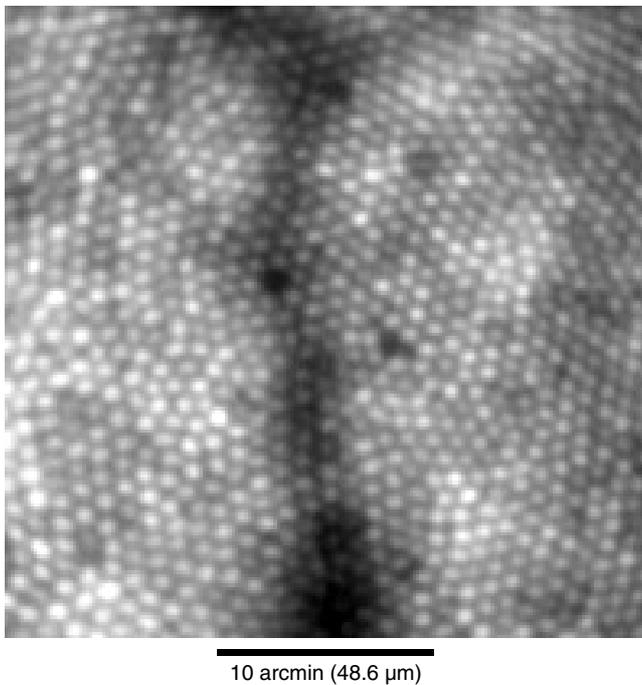
Sampling by the Photoreceptor Mosaic

The retina is lined by millions of tiny cells, called photoreceptors, that sample the image that reaches the retina. Unlike a CCD camera, this array is far from uniform. Each photoreceptor is a like a fiber-optic waveguide that funnels the light into its outer segment, which is filled with photosensitive pigment. Rod photoreceptors make up by far the majority of the photoreceptors, totaling more than 100 million in a typical human retina. These cells are very sensitive and can signal the absorption of a single photon. Cone photoreceptors are less sensitive than rods and come in three types, each sensitive to a different portion of the visible light spectrum. The combined signals from the three cone-types provide color vision to the human eye at high light levels. There are only about 5 million cones, and they are most dense
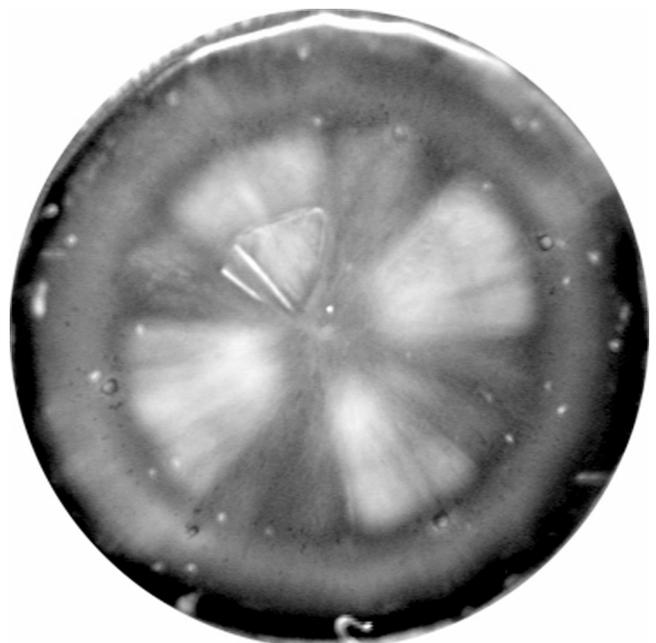
Figure 15. This picture shows the Maltese cross appearance of the isolated crystalline monkey lens when viewed by a polarizer-analyzer combination. The pattern arises because of the birefringent structures in the lens. (Courtesy of Adrian Glasser and Austin Roorda).
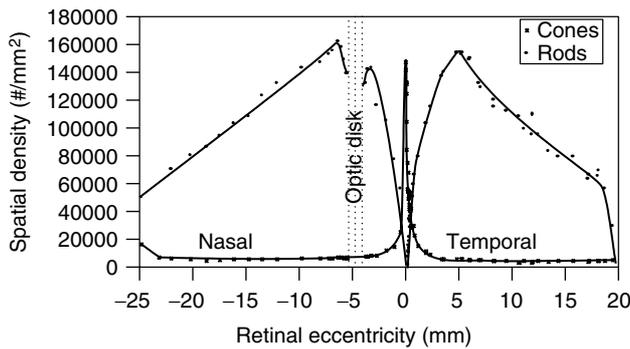
Figure 16. This classic figure generated from Østerberg's data shows the spatial density of rods and cones in the human retina. It illustrates the extreme nonuniformity of photoreceptor distributions across the retina. Only cones comprise the fovea, but rods quickly dominate outside that area. The decrease in spatial density toward the periphery occurs because of an increase in photoreceptor size with eccentricity (generated from Table 3 in (154)].

10 arcmin (48.6 µm)

Figure 17. The photoreceptor mosaic shown here was taken of a living human retina using an adaptive optics ophthalmoscope (155). This image shows photoreceptors at a location 1° from the foveal center. The cones are about 5 microns in diameter and are packed into a quasi-crystalline array. Rods are also present in this portion of the retina, but they were too small to be resolved by the ophthalmoscope (courtesy of Austin Roorda and David Williams).

near the posterior pole of the eyeball in an area called the macula, which contains the fovea. The density of cones and rods across the retina is illustrated in Fig. 16. An actual image of the photoreceptor array in a living human eye is shown in Fig. 17. Circuitry in the retina transforms signals from the photoreceptors into a compact representation of color and luminance across the visual field. In fact, the

number of wires (optic nerves) that carries the signal to the brain totals only 1.2 million. This reduction is accomplished by devoting only a disproportionate amount of wiring to a small region of the retina called the fovea, which is comprised only of cones. The number of optic nerves for each cone in the fovea is estimated to be from two to four (126,127). Across the rest of the retina, signals from individual rod and cone photoreceptors are pooled together, thereby reducing the number of dedicated optic nerves. The impressive feature of the human retina is that it offers both high visual acuity and a large field of view and uses fewer fibers than there are pixels in a modern CCD camera!

The nature of the detecting surface is very important for vision because the sampling array imposes a final limit on what is seen and not seen by the human eye. Nyquist's sampling theorem states that to measure a spatially varying signal properly, one must sample it at twice the frequency. In the human retina, the density of the sampling is greatest at the fovea, where there is one optic nerve for each photoreceptor. The typical packing density of cones in the human fovea is about 199,000 cones per mm^2 (128). This converts to a lateral sampling density of 480 cycles/mm or 140 cycles/degree. [NOTE: In vision science, space is often represented in degrees because its value is the same in object space as in image space.] Given this sampling density, the maximum spatial frequency that the eye could resolve would be 70 cycles/degree. To measure this property, investigators had to project spatial frequency patterns on the retina that were unaffected by the optics of the eye. This was done by projecting interference fringes directly onto the retina via two tiny, mutually coherent entrance beams (129,130). The interferometric technique is simply Young's double-slit phenomenon where the fringes are projected directly onto the retina. This technique has been used since to isolate effectively the optical and neural factors affecting vision (12,131,132).

The human retina is very economical in design. It has a sampling array that is just high enough to detect the spatial frequencies that the optical system can transmit to the retina. For example, the cutoff spatial frequency of a 2-mm pupil for 550 nm light is 77 cycles/degree. This is closely matched to the maximum frequency that the retina is equipped to detect. For larger pupil sizes, the cutoff would increase linearly, but because of aberrations, the practical spatial frequency cutoff does not increase (13).

At retinal locations away from the fovea, the sampling density drops off precipitously due to an increase in photoreceptor size and a decrease in the *optic nerves:photoreceptor* ratio. To deal with this drop-off in vision, the eye (and head) is equipped with muscles that allow us to align objects of regard so that their images always land on the fovea.
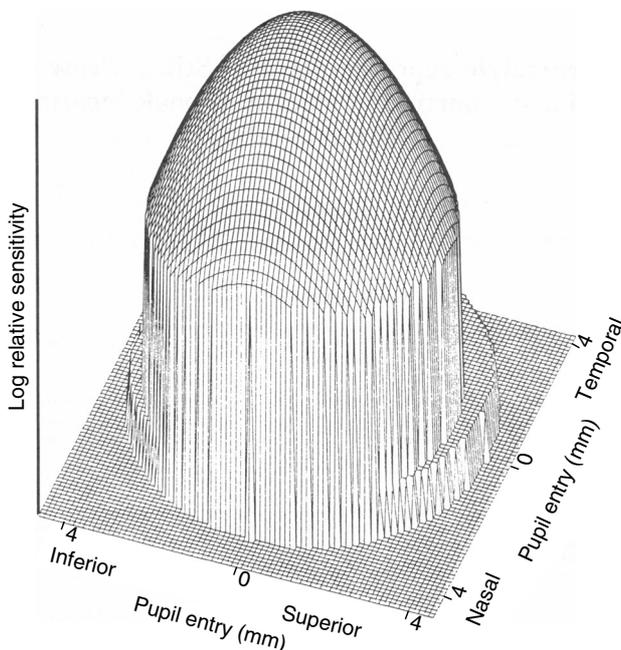
The Stiles–Crawford Effect

Rod and cone photoreceptors act as fiber-optic waveguides. Because they are optical waveguides, they have angular tuning properties. In the human eye, these properties give rise to both perceptual and reflective effects, which

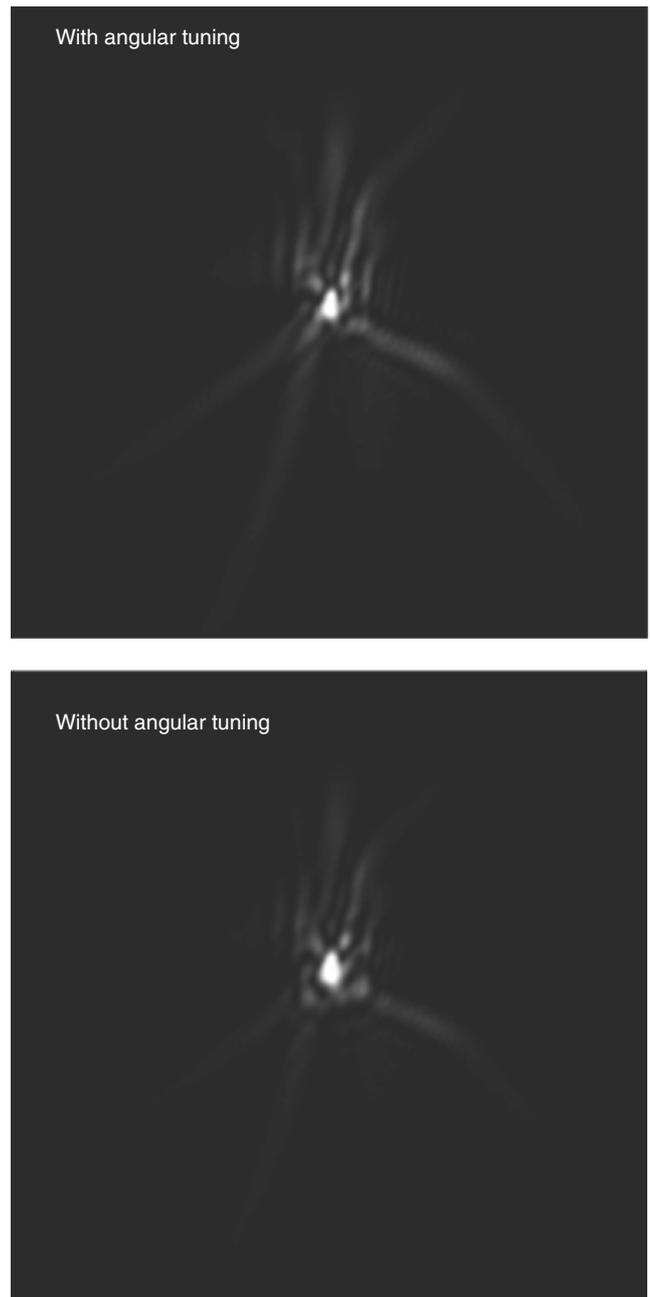are important for vision and for imaging of the retina, respectively.

The perceptual effect, called the Stiles−Crawford effect, describes the change in the perceived brightness of light as a function of the pupil location at which the light enters. (Changing the pupil location of the entrance beam changes the angle at which the incident light strikes the photoreceptor.) The tuning is sensitive enough that the angular sensitivity reduces to about half at the edge of a 8-mm pupil (see Figure 18) (133).

The reflected light from the photoreceptors has similar directional properties. If the light emerging from the eye from a small illuminated patch of retina is measured as a function of pupil position, the reflectance is highest near the center of the pupil (134−138).

Directional effects on the way into and out of the eye play an important role in determining image quality in the human eye. Although the optical system will produce a point spread on the retina, the retina preferentially accepts that portion of the PSF that is generated by the more central rays. It is hypothesized that the reason for this angular tuning is to suppress the contribution from the more aberrated peripheral rays in the optics to improve image quality. The expected improvements near best focus are quite small (139), but Zhang et al. showed that for defocused images, the Stiles−Crawford effect tends to increase depth of focus and prevent phase reversals (140). For imaging, the light emerging from the eye will always be weighted more for central rays than for peripheral rays.

Figure 19. We calculated the PSF of a typical human eye with and without incorporating the Stiles−Crawford effect in the calculation. PSFs were calculated for 550-nm light over a 7-mm pupil at the focal plane that had the highest Strehl ratio. The tuning value we chose was $\rho = 0.047$ mm^{-1}. The angular tuning has the effect of apodizing rays from the margins of the pupil. The result is that high spatial frequencies in the PSF are attenuated and low spatial frequencies are enhanced.

Figure 18. The optical fiber properties of the photoreceptors give rise to a perceived phenomenon called the Stiles−Crawford effect. This plot shows the log relative sensitivity of the eye to light for changing pupil entry positions. Changing pupil entry position is the method used to change the angle of the incident beam on the retina. The sensitivity to light reduces to about half at the edges of an 8-mm pupil [Reproduced from Fig. 1 in (133)].

A simple way to incorporate these angular tuning effects into computations for image quality is to project the tuning properties into the pupil function [see Eq. (1)]. A detector that has an angular tuning function that has reduced light sensitivity to light emerging from the edge of the pupil is, in effect, the same as a uniformly sensitive detector that has a pupil that has reduced transmission
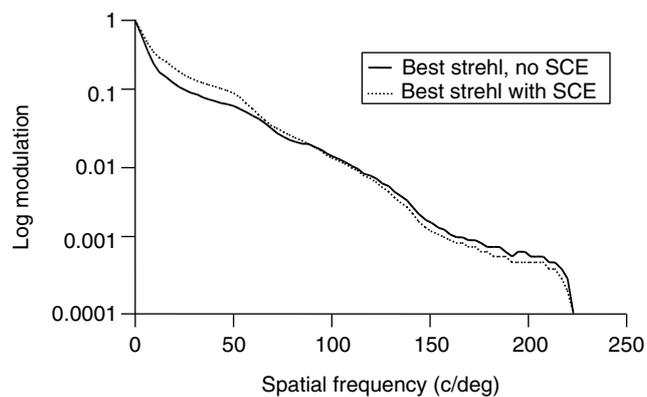
at its edges. Likewise, light reflected from the retina that is preferentially directed toward the center of the exit pupil can be modeled as light from a uniformly reflecting retina passing through a pupil where absorbance increases toward the periphery.

Figure 19 shows the computed PSF of an eye that has typical aberrations before and after angular tuning is incorporated into the pupil function. Figure 20 shows the corresponding average radial MTFs for the same pupil functions.
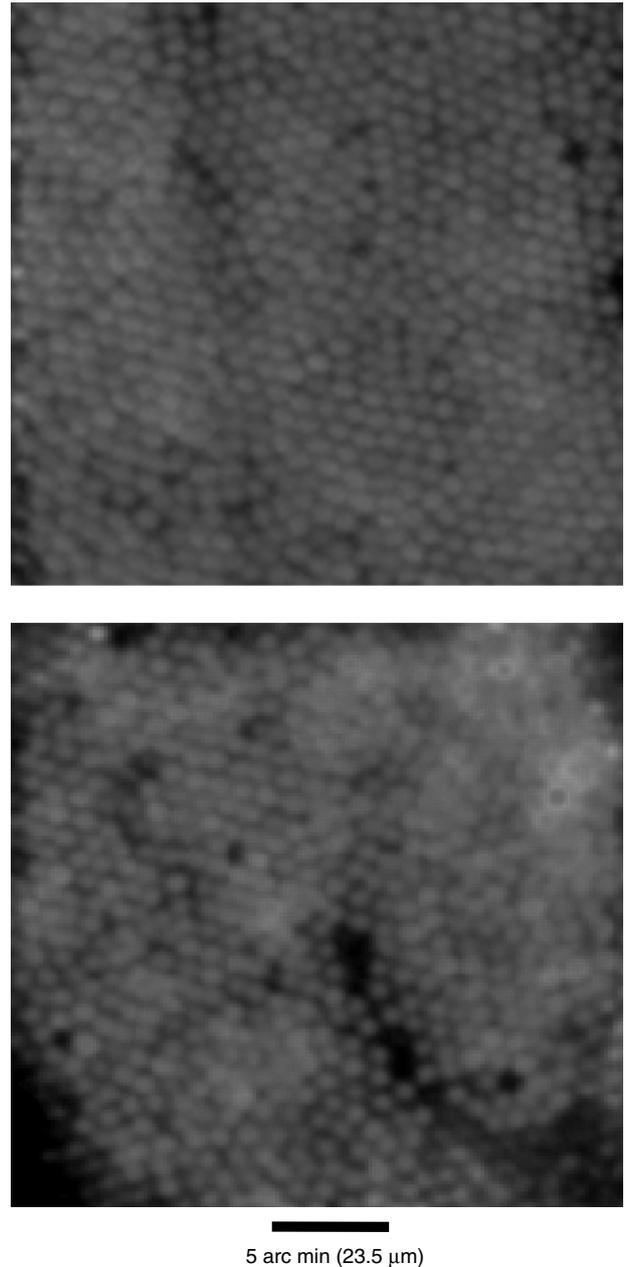
Chromatic Sampling of the Retinal Image

There are three types of cone photoreceptors; long (L), middle (M), and short (S) wavelength-sensitive cones. These are arranged in a single plane on the retina, and therefore, chromatic sampling on the retina is worse than spatial sampling. The S cones comprise only about 5% of the cones and thus are poor at spatial tasks. Furthermore, there are no S cones in the fovea. Without S cones, the eye confuses the distinction between blue and yellow in a condition called tritanopia. For this reason, the region around the fovea that is devoid of S cones is called the tritanopic zone. In the periphery, the S cones approach a partially crystalline arrangement (141) to achieve relatively uniform coverage.

L and M cones comprise the remaining 95% of the cones in the retina; recent measurements have shown that these cones are randomly distributed in the retina (142,143). (see Fig. 21). This arrangement leaves the eye locally color-blind over patches as large as 5 minutes of arc. This phenomena goes largely unnoticed, but it is likely that it is one of the factors that
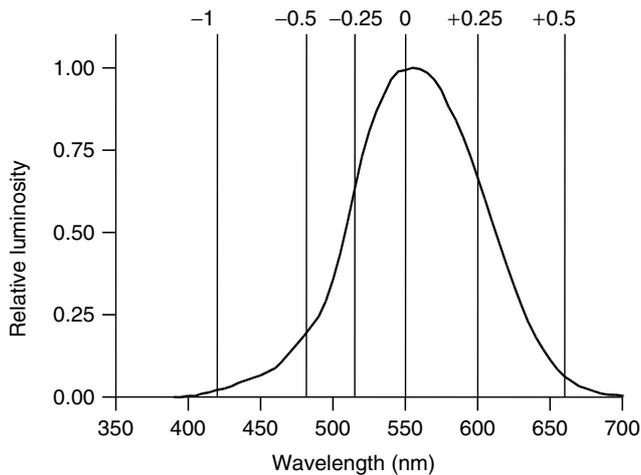

5 arc min (23.5 μm)

Figure 21. Pseudocolor images of the trichromatic cone mosaic in two human eyes. Blue, green, and red colors represent the short (S), middle (M), and long (L) wavelength-sensitive cones, respectively. The two human subjects have a more than threefold difference in the number of L vs. M cones (142), yet both eyes have essentially the same color vision (156). In both mosaics shown, the arrangement of the S, M, and L cones is essentially random (143). See color insert.

gives rise to the blotchy colored appearance of high-spatial-frequency gratings, a phenomena called Brewster's colors (144).

The Spectral Luminosity Function and Chromatic Aberration

The combination of cone photopigments, adaptation, absorption, and retinal wiring limits the spectral response to wavelengths that make up the visible spectrum. The

Figure 20. The MTFs in this plot show the spatial-frequency-dependent effects of pupil apodization via cone angular tuning. When angular tuning is incorporated in calculations of the PSF in the focal plane that has the highest Strehl ratio, the contrasts for spatial frequencies that the eye can see (60 c/deg and below) are enhanced and higher spatial frequencies are attenuated. Therefore, the retinal image quality for a large pupil is improved and, at the same time, aliasing effects due to the presence of spatial frequencies beyond the eye's maximum detectable spatial frequency are reduced. The SCE used $\rho = 0.047$ mm^{-1} and PSF calculations were done over a 7-mm pupil for a single eye. Incidentally, similar calculations of the MTF in the focal plane that had the lowest rms aberration show less of an effect.

Figure 22. The spectral luminosity function of the eye limits the deleterious effect of chromatic aberration. This figure shows that if 550-nm light is in focus, more than 70% of the energy detected in the white light spectrum is within +/− 0.25 D of defocus. One-quarter of a diopter is considered a tolerable defocus for a human eye under typical conditions [after Fig. 3 in (145)].

exact spectrum to which we are sensitive depends on light levels. Because rods saturate at moderate and high light levels, cones largely govern the spectral sensitivity in that region. Because the more numerous M and L cones also mediate luminance, the spectral sensitivity function is weighted toward their end of the spectrum. This spectrum is referred to as the *photopic luminous efficiency function*. For lower light levels, cones lose sensitivity and rods, which are no longer saturated, dominate the response. At the lowest light levels, the spectral sensitivity curve is called the *scotopic luminous efficiency function*. The narrow spectral range of both of these functions filters some of the effects of chromatic aberration. Recall previously that the amount of chromatic aberration in the eye was about 2.2 D from 400 to 700 nm. This degree of chromatic aberration of the eye would normally be deleterious for image quality, but the severity of the chromatic aberration is lessened because the eye has a tuned spectral bandwidth. Thibos et al. illustrate this well in Fig. 22 showing that although the longitudinal chromatic aberration is 2 D, more than 70% of the luminous energy is confined to a defocus range of less than 0.25 D defocus on either side of focus, provided that the eye is optimally focused at 550 nm (145).

An analysis of the optical quality of the eye in frequency space using the MTF further demonstrates that chromatic aberration contributes surprisingly little to image degradation in the eye. By calculating the MTF as a function of chromatic defocus and generating the white light MTF as a sum of all visible wavelengths, weighted by the luminance spectrum, Thibos et al. found that the uncorrectable blur due to chromatic aberration is equivalent to a monochromatic defocus of less than 0.2 D for an eye that has a 2.5-mm pupil, a tolerable amount of defocus in a human eye (145). These predictions support the earlier work

of Campbell and Gubisch who found that contrast sensitivity improved by less than 0.2 log units across 10−40 cycles per degree of spatial frequencies when using monochromatic light (146). For large pupils, the image degradation is expected to be greater, but increased depth of focus that arises from the presence of monochromatic aberrations tends to reduce these deleterious effects (147).

BIBLIOGRAPHY

1. G. B. Benedek, *Appl. Opt.* **10**(3), 459−473 (1971).
2. J. Liang, B. Grimm, S. Goelz, and J. F. Bille, *J. Opt. Soc. Am. A* **11**, 1,949−1,957 (1994).
3. L. N. Thibos and X. Hong, *Optometry Vision Sci.* **76**(12), 817−825 (1999).
4. W. N. Charman and J Cronly-Dillon, eds., *Visual Optics and Instrumentation*, CRC Press, Boca Raton, 1991, p. 1−26.
5. H. C. Howland, J. Buettner, and R. A. Applegate, *Vision Sci. Appl. Tech. Dig.* **2**, 54−57 (1994).
6. J. Schwiegerling and J. E. Greivenkamp, *Optometry Vision Sci.* **74**(11), 906−916 (1997).
7. T. Oshika et al., *Am. J. Ophthalmol.* **127**(1), 1−7 (1999).
8. K. M. Oliver et al., *J. Refract. Surg.* **13**(3), 246−254 (1997).
9. R. A. Applegate and H. C. Howland, *J. Refract. Surg.* **13**, 295−299 (1997).
10. R. A. Applegate et al., *J. Refract. Surg.* **16**, 507−514 (2000).
11. E. Moreno-Barriuso et al., *Invest. Ophthalmol. Vision Sci.* **42**(6), 1,396−1,403 (2001).
12. F. W. Campbell and D. G. Green, *J. Physiol.* **181**, 576−593 (1965).
13. F. W. Campbell and R. W. Gubisch, *J. Physiol.* **186**, 558−578 (1966).
14. J. Liang and D. R. Williams, *J. Opt. Soc. Am. A* **14**(11), 2,873−2,883 (1997).
15. H. Helmholtz and J. P. C. Southall, eds., *Helmholtz's Treatise on Physiological Optics*, Optical Society of America, Rochester, 1924.
16. A. Glasser and M. C. W. Campbell, *Vision Res.* **39**, 1,991−2,015 (1999).
17. D. A. Atchison, *Ophthal. Physiol. Opt.* **15**(4), 255−272, (1995).
18. A. Glasser and M. C. W. Campbell, *Vision Res.* **38**(2), 209−229 (1998).
19. A. Duane, *JAMA* **59**, 1,010−1,013, (1912).
20. J. R. Kuszak, B. A. Bertram, M. S. Macsai, and J. L. Rae, *Scanning Electron Micros.* **3**, 1,369−1,378 (1984).
21. J. R. Kuszak, K. L. Peterson, J. G. Sivak, and K. L. Herbert, *Exp. Eye Res.* **59**, 521−35 (1994).
22. T. Young, *Philos. Trans. R. Soc. London* **91**, 23−88 (1801).
23. L. Matthiessen, *Pflügers Archiv* **27**, 510−523 (1882).
24. J. C. Maxwell, *Cambridge and Dublin Math. J.* **8**, 188−195 (1854).
25. M. C. W. Campbell, *Vision Res.* **24**(5), 409−415 (1984).
26. R. H. H. Kröger, M. C. W. Campbell, and R. Munger, *Vision Res.* **34**(14), 1,815−1,822 (1994).
27. B. K. Pierscionek and D. Y. C. Chan, *Optometry Vision Sci.* **66**(12), 822−829 (1989).
28. M. C. W. Campbell and A. Hughes, *Vision Res.* **21**, 1,129−1,148 (1981).

29. L. F. Garner and G. Smith, *Optometry Vision Sci.* **74**(2), 114–119 (1997).

30. D. A. Atchison and G. Smith, *Optics of the Human Eye*, Butterworth-Heinemann, Oxford, 2000.

31. M. Tscherning and C. Weiland, eds., *Physiologic Optics*, 4th ed., Keystone Publishing Co., Philadelphia, 1924.

32. C. Cui and V. Lakshminarayanan, *J. Opt. Soc. Am. A* **15**(9), 2,488–2,496 (1998).

33. A. G. Bennett and R. B. Rabbetts, *Clinical Visual Optics*, 2nd ed., Butterworths, London, 1989.

34. T. C. A. Jenkins, *Br. J. Physiol. Opt.* **20**, 59–91 (1963).

35. R. E. Scammon and M. B. Hesdorffer, *Arch. Ophthalmol.* **17**, 104–112 (1937).

36. R. A. Weale, *Nature* **198**, 944–946 (1963).

37. A. Guirao, M. Redondo, and P. Artal, *J. Opt. Soc. Am. A* **17**(10), 1,697–1,702 (2000).

38. P. Artal, A. Guirao, and D. R. Williams, *Invest. Ophthalmol. Vision Sci. Suppl.* **40**(4), 39 (1999).

39. H. C. Howland and B. Howland, *J. Opt. Soc. Am.* **67**, 1,508–1,518 (1977).

40. M. S. Smirnov, *Biophysics* **6**, 776–795 (1962).

41. M. CW. Campbell, E. M. Harrison, and P. Simonet, *Vision Res.* **30**, 1,587–1,602 (1990).

42. R. H. Webb, M. Penney, and K. P. Thompson, *Appl. Opt.* **31**, 3,678–3,686 (1992).

43. R. Navarro and M. A. Losada, *Vision Sci. Appl: Tech. Dig.* **1**, 230–233 (1996).

44. G. Walsh, W. N. Charman, and H. C. Howland, *J. Opt. Soc. Am. A* **1**, 987–992 (1984).

45. W. S. Stiles and B. H. Crawford, *Proc. R. Soc. London B.* **112**, 428–450 (1933).

46. D. Malacara, S. L. DeVore, and D. Malacara, eds., *Optical Shop Testing*, 2nd ed., Wiley-Interscience, New York, 1996, pp. 455–499.

47. J. W. Goodman, *Introduction to Fourier Optics*, McGraw-Hill, New York, 1968.

48. L. N. Thibos, R. A. Applegate, J. Schwiegerling, and R. H. Webb, and VSIA Standards Taskforce Members, V. Lakshminarayanan, ed., Standards for Reporting the Optical Aberrations of Eyes, Optical Society of America, Washington, DC, 232–235 2000.

49. M. A. Wilson, M. CW. Campbell, and P. Simonet, *Optometry Vision Sci.* **69**, 129–136 (1992).

50. G. Walsh, *Ophthal. Physiol. Opt.* **8**, 178–181 (1988).

51. H. J. Wyatt, *J. Ocular Pharmacol. Ther.* **12**(4), 441–459 (1996).

52. R. Bracewell, *The Fourier Transform and its Applications*, McGraw-Hill, New York, 1965.

53. A. Guirao and D. R. Williams, *Invest. Ophthalmol. Vision Sci. Suppl.* **42**(4), 98 (2001).

54. D. C. Knill, D. Field, and D. Kersten, *J. Opt. Soc. Am. A* **7**(6), 1,113–1,123 (1990).

55. D. J. Field and N. Brady, *Vision Res.* **37**(23), 3,367–3,383 (1997).

56. S. Marcos, S. A. Burns, E Moreno-Barriuso, and R. Navarro, *Vision Res.* **39**, 4,309–4,323 (1999).

57. P. Simonet and M. C. W. Campbell, *Vision Res.* **30**(2), 187–206 (1990).

58. L. N. Thibos et al., *Vision Res.* **30**(1), 33–49 (1990).

59. M. Rynders, B. Lidkea, W. Chisholm, and L. N. Thibos, *J. Opt. Soc. Am. A* **12**(10), 2,348–2,357 (1995).

60. G. Westheimer, *Vision Res.* **22**, 157–162 (1982).

61. E. Jackson, *Trans. Am. Ophthalmol. Soc.* **5**, 141–149 (1888).

62. M. Koomen, R. Tousey, and R. Scolnik, *J. Am. Opt. Assoc.* **39**, 370–376 (1949).

63. A. Ivanoff, *J. Opt. Soc. Am.* **46**, 901–903 (1956).

64. G. van den Brink, *Vision Res.* **2**, 233–244 (1962).

65. F. Berny, S. Slansky, J Home Dickon, eds., *Optical Instruments and Techniques*, Oriel Press, London, pp. 375–385 1969.

66. J. Santamaria, P. Artal, and J. Bescos, *J. Opt. Soc. Am. A* **4**, 1,109–1,114 (1987).

67. J. C. He, S. Marcos, R. H. Webb, and S. A. Burns, *J. Opt. Soc. Am. A* **15**(9), 2,449–2,457 (1998).

68. I. Iglesias, E. Berrio, and P. Artal, *J. Opt. Soc. Am. A* **15**(9), 2,466–2,476 (1998).

69. T. Salmon, L. N. Thibos, and A. Bradley, *J. Opt. Soc. Am. A* **15**(9), 2,457–2,465 (1998).

70. A. Guirao and P. Artal, *Vision Res.* **39**, 207–217 (1999).

71. D. R. Williams et al., *Vision Res.* **36**(8), 1,103–1,114 (1996).

72. J. A. M. Jennings and W. N. Charman, *Vision Res.* **21**, 445–455 (1981).

73. P. Artal, A. M. Derrington, and E. Colombo, *Vision Res.* **35**(7), 939–947 (1995).

74. W. Lotmar and T. Lotmar, *J. Opt. Soc. Am.* **64**(4), 510–513 (1974).

75. M. Millodot and A. Lamont, *J. Opt. Soc. Am.* **64**, 110–111 (1974).

76. F. Rempt, J. Hoogerheide, and W. P. H. Hoogenboom, *Ophthalmologica* **162**, 1–10 (1971).

77. C. E. Ferree, G. Rand, and C. Hardy, *Arch. Ophthalmol.* **5**, 717–731 (1931).

78. P. Artal, S. Marcos, R. Navarro, and D. R. Williams, *J. Opt. Soc. Am. A* **12**, 195–201 (1995).

79. A. Roorda and M. C. W. Campbell, *Invest. Ophthalmol. Vision Sci. Suppl.* **35**, 1,258 (1994).

80. R. Navarro, E. Moreno, and C. Dorronsoro, *J. Opt. Soc. Am. A* **15**(9), 2,522–9 (1998).

81. A. Roorda and W. R. Bobier, *J. Opt. Soc. Am. A* **13**, 3–11 (1996).

82. P. Artal and R. Navarro, *Appl. Opt.* **31**, 3,646–3,456 (1992).

83. D. A. Atchison et al., *Vision Res.* **35**, 313–323 (1995).

84. C. Lu, M. CW. Campbell, and R. Munger, *Ophthalmic Visual Opt. Tech. Dig.* **3**, 160–163 (1994).

85. J. C. He, S. A. Burns, and S. Marcos, *Vision Res.* **40**(1), 41–48 (2000).

86. A. Glasser and M. CW. Campbell, *Vision Sci. Appl.: Tech. Dig.* **1**, 246–249 (1996).

87. H. Hofer, J. Porter, and D. R. Williams, *Invest. Ophthalmol. Vision Sci. Suppl.* **39**(4), 203 1998.

88. M. Mrochen, M. Kaemmerer, and T. Seiler, *J. Refract. Surg.* **16**, 116–121 (2000).

89. P. Artal and A. Guirao, *Opt. Lett.* **23**, 1,713–1,715 (1998).

90. H. Hofer, P. Artal, J. L. Aragon, and D. R. Williams, *J. Opt. Soc. Am. A* **18**(3), 497–506 (2001).

91. P. Artal, A. Guirao, E. Berrio, and D. R. Williams, *Invest. Ophthalmol. Vision Sci. Suppl.* **42**(4), 895 (2001)

92. T. Salmon and L. N. Thibos, [Abstract] *OSA Annu. Meet. Tech. Dig.* p. 70 1998.

93. D. Bartsch, G. Zinser, and W. R. Freeman, *Vision Sci. Appl.: Tech. Dig.* pp. 134–137 1994.

94. J. C. He et al., *Myopia 2000 Meet.*, Boston, July, 2000; S. Marcos et al., *ibid.*; X. Cheng et al., *ibid.*; M. C. W. Campbell et al., *ibid*.

95. M. J. Collins, C. F. Wildsoet, and D. A. Atchison, *Vision Res.* **35**, 1,157–1,163 (1995).

96. D. Whitaker, R. Steen, and D. B. Elliot, *Optometry Vision Sci.* **70**(11), 963–968 (1993).

97. T. J. van den Berg, *Invest. Ophthalmol. Vision Sci.* **38**(7), 1,321–1,332 (1997).

98. J. J. Vos, *CIE J.* **3**(2), 39–53 (1984).

99. W. S. Stiles, *Proc. R. Soc. London B* **104**, 322–355 (1929).

100. L. L. Holladay, *J. Opt. Soc. Am.* **12**, 271–319 (1926).

101. M. L. Hennelly, J. L. Barbur, D. F. Edgar, and E. G. Woodward, *Ophthalmol. Physiol. Opt.* **18**(2), 197–203 (1998).

102. J. K. Ijspeert, P. W. de Waard, T. J. van den Berg, and P. T. de Jong, *Vision Res.* **30**(5), 699–707 (1990).

103. D. van Norren and J. J. Vos, *Vision Res.* **14**, 1,237–1,244 (1974).

104. E. A. Boettner and J. R. Wolter, *Invest. Ophthalmol. Vision Sci.* **1**(6), 776–783 (1962).

105. G. L. Savage, G Haegerstrom-Portnoy, A. J. Adams, and S. E. Hewlett, *Clin. Vision. Sci.* **8**(1), 97–108 (1993).

106. J. Pokorny, V. C. Smith, and M. Lutze, *Appl. Opt.* **26**(8), 1,437–1,440 (1987).

107. F. C. Delori and S. A. Burns, *J. Opt. Soc. Am. A* **13**(2), 215–226 (1996).

108. D. M. Snodderly, R. S. Weinhaus, and J. C. Choi, *J. Neuroscience* **12**(4), 1,169–1,193 (1992).

109. O. Sommerburg, J. E. Keunen, A. C. Bird, and F. J. van Kuijk, *Br. J. Ophthalmol.* **82**(8), 907–910 (1998).

110. P. Pease, A. J. Adams, E. Nuccio, *Vision Res.* **5**, 705–710 (1973).

111. D. M. Snodderly, J. D. Auran, and F. C. Delori, *Invest. Ophthalmol. Vision Sci.* **25**(6), 674–685 (1984).

112. B. R. J. Hammond, B. R. Wooten, and D. M. Snodderly, *Vision Res.* **36**(18), 3,003–3,009 (1996).

113. B. R. J. Hammond, B. R. Wooten, and D. M. Snodderly, *J. Opt. Soc. Am. A* **14**(6), 1,187–1,196 (1997).

114. J. T. Landrum, R. A. Bone, and M. D. Kilburn, *Adv. Pharmacol.* **38**, 537–556 (1997).

115. B. R. J. Hammond, B. R. Wooten, and D. M. Snodderly, *Invest. Ophthalmol. Vision Sci.* **39**, 397–406 (1998).

116. D. M. Snodderly, P. K. Brown, F. C. Delori, and J. D. Auran, *Invest. Ophthalmol. Vision Sci.* **25**(6), 660–673 (1984).

117. A. Stanworth and E. Naylor, *Br. J. Ophthalmol.* **34**, 201–211 (1950).

118. G. J. van Blokland and S. C. Verhelst, *J. Opt. Soc. Am. A* **4**, 82–90 (1987).

119. C. C. D. Shute, *Nature* **250**, 163–164 (1974).

120. D. J. Donohue, B. J. Stoyanov, R. L. McCally, and R. A. Farrel, *Cornea* **15**(3), 278–285 (1996).

121. D. J. Donohue, B. J. Stoyanov, R. L. McCally, and R. A. Farrel, *J. Opt. Soc. Am. A* **12**(7), 1,425–1,438 (1995).

122. J. M. Bueno and P. Artal, *J. Opt. Soc. Am. A* **18**(3), 489–496 (2001).

123. J. M. Bueno, *Vision Res.* **40**(28), 3,791–3,799 (2000).

124. F. A. Bettelheim, *Exp. Eye Res.* **21**, 231–234 (1975).

125. D. G. Cogan, *Arch. Ophthalmol.* **25**(3), 391–400 (1941).

126. C. A. Curcio and K. A. Allen, *J. Comp. Neurol.* **300**, 5–25 (1990).

127. J. Sjostrand, N. Conradi, and L. Klarén, *Graefe's Arch. Clin. Exp. Ophthalmol.* **232**, 432–437 (1994).

128. C. A. Curcio, K. R. Sloan, R. E. Kalina, and A. E. Hendrickson, *J. Comp. Neurol.* **292**, 497–523 (1990).

129. G. Westheimer, *J. Physiol.* **152**, 67–74 (1960).

130. M. A. Arnulf and M. O. Dupuy, *C. R. Acad. Sci. (Paris)* **250**, 2,757–2,759 (1960).

131. D. R. Williams, *Vision Res.* **28**, 433–454 (1988).

132. D. R. Williams, D. Brainard, M. J. McMahon, and R. Navarro, *J. Opt. Soc. Am. A* **11**, 3,123–3,135 (1994).

133. R. A. Applegate and V. Lakshminarayanan, *J. Opt. Soc. Am. A* **10**(7), 1,611–1,623 (1993).

134. J. -M. Gorrand, *Vision Res.* **19**, 907–912 (1979).

135. J. -M. Gorrand, *Ophthalmol. Physiol. Opt.* **9**, 53–60 (1989).

136. J. -M. Gorrand, R. Alfieri, J. -Y. Boire, *Vision Res.* **24**, 1,097–1,106 (1984).

137. G. J. van Blokland, *Vision Res.* **26**, 495–500 (1986).

138. S. A. Burns, S. Wu, F. C. Delori, and A. E. Elsner, *J. Opt. Soc. Am. A* **12**, 2,329–2,338 (1995).

139. D. A. Atchison, D. H. Scott, A. Joblin, and G. Smith, *J. Opt. Soc. Am. A* **18**(6), 1,201–1,211 (2001).

140. X. Zhang, M. Ye, A. Bradley, and L. N. Thibos, *J. Opt. Soc. Am. A* **16**(4), 812–820 (1999).

141. K. Bumstead and A. Hendrickson, *J. Comp. Neurol.* **403**, 502–516 (1999).

142. A. Roorda and D. R. Williams, *Nature* **397**, 520–522 (1999).

143. A. Roorda, A. B. Metha, P. Lennie, and D. R. Williams, *Vision Res.* **41**(12), 1,291–1,306 (2001).

144. Brewster D., *London Edinboro Philos. Mag. J. Sci.* **1**, 169–174 (1832).

145. L. N. Thibos, A. Bradley, and X. X. Zhang, *Optometry Vision Sci.* **68**(8), 599–607 (1991).

146. F. W. Campbell and R. W. Gubisch, *J. Physiol.* **192**, 345–358 (1967).

147. G. Yoon, I. Cox, and D. R. Williams, *Invest. Ophthalmol. Vision Sci. Suppl.* **40**(4), 40 (1999).

148. S. A. Strenk et al., *Invest. Ophthalmol. Vision Sci.* **40**(6), 1,162–1,169 (1999).

149. G. Wald and D. R. Griffin, *J. Opt. Soc. Am.* **37**, 321–336 (1947).

150. R. E. Bedford and G. Wyszecki, *J. Opt. Soc. Am.* **47**, 564–565 (1957).

151. A. Ivanoff, *C. R. Acad. Sci.* **223**, 170–172 (1946).

152. I. Iglesias, N Lopez-Gill, P. Artal, *J. Opt. Soc. Am. A* **15**(2), 326–339 (1998).

153. R. I. Calver, M. J. Cox, and D. B. Elliot, *J. Opt. Soc. Am. A* **16**(9), 2,069–2,078 (1999).

154. G. Østerberg, *Acta Ophthalmologica* Suppl. **6**, 1–103 (1935).

155. J. Liang, D. R. Williams, and D. Miller, *J. Opt. Soc. Am. A* **14**(11), 2,884–2,892 (1997).

156. D. H. Brainard et al., *J. Opt. Soc. Am. A* **17**(3), 607–614 (2000).

157. M. Born and E. Wolf, *Principles of Optics*, Pergamon Press, New York, 1980.

158. L. J. Bour and N. J. Lopes Cardozo, *Vision Res.* **21**, 1,413–1,421 (1981).

159. D. Kaplan and F. A. Bettelheim, *Exp. Eye Res.* **13**, 219–226 (1972).

160. D. Post and G. E. Gurland, *Exp. Eye Res.* **5**, 286–295 (1966).